Accepted Manuscript

Matching of kinetics of $CaCO_3$ decomposition and CuO reduction with CH_4 in Ca-Cu chemical looping

Changlei Qin, Bo Feng, Junjun Yin, Jingyu Ran, Li Zhang, Vasilije Manovic

PII: S1385-8947(14)01351-5
DOI: http://dx.doi.org/10.1016/j.cej.2014.10.030
Reference: CEJ 12773

To appear in: *Chemical Engineering Journal*

Received Date: 7 August 2014
Revised Date: 7 October 2014
Accepted Date: 9 October 2014

Please cite this article as: C. Qin, B. Feng, J. Yin, J. Ran, L. Zhang, V. Manovic, Matching of kinetics of $CaCO_3$ decomposition and CuO reduction with CH_4 in Ca-Cu chemical looping, *Chemical Engineering Journal* (2014), doi: http://dx.doi.org/10.1016/j.cej.2014.10.030

Matching of kinetics of $CaCO_3$ decomposition and CuO reduction with CH_4 in Ca-Cu chemical looping

Changlei Qin,[a,b] *Bo Feng,*[c] *Junjun Yin,*[c] *Jingyu Ran,*[a,b] *Li Zhang,*[a,b] *and Vasilije Manovic* *[d]

[a] Key Laboratory of Low-grade Energy Utilization Technologies and Systems of Ministry of Education, Chongqing University, Chongqing 400044, China

[b] College of Power Engineering, Chongqing University, Chongqing 400044, China

[c] School of Mechanical and Mining Engineering, The University of Queensland, St Lucia, Queensland 4072, Australia

[d] School of Engineering, Cranfield University, Cranfield, Bedfordshire MK43 0AL, United Kingdom

*Corresponding author:

Email: c.qin@cqu.edu.cn (Changlei Qin); v.manovic@cranfield.ac.uk (Vasilije Manovic).

ABSTRACT

Ca-Cu chemical looping (CaL-CLC) based on calcium looping is a novel and promising process for CO_2 capture. The concept utilizes the heat released from the exothermic reduction of CuO to support the endothermic regeneration of CaO-based sorbents. Therefore, it is important for the two major reactions to have matching kinetics. This work assesses kinetics of the two reactions in a calciner under the conditions of interest for CaL-CLC. The reaction rates of the decomposition of $CaCO_3$ and reduction of CuO-based material with CH_4 were measured in a TGA by varying the temperature and gas atmosphere, and two gas-solid reaction models were utilized for the determination of the kinetic parameters. On the basis of these results, a dynamic model was developed to investigate the simultaneous reduction of CuO and decomposition of $CaCO_3$ in an adiabatic fixed-bed reactor operating at 1 atm. The simulation results showed that the reduction of CuO completed extremely fast under all test conditions, and it could lead to hot spots in the calciner. It was found that addition of steam into the reducing gas could enhance the reaction rate of $CaCO_3$ decomposition and help it match the fast rate of CuO reduction, then reduce the formation of hot spots. Also, steam could be used to control the movement of reaction front. Although CO_2 could be used to control the reaction front as well, the higher CO_2 partial pressure in CH_4 was found to slow down the decomposition of $CaCO_3$ leading to incomplete reaction.

Keywords: CO_2 capture; Kinetic matching; CuO reduction with CH_4; $CaCO_3$ decomposition; Ca-Cu chemical looping

1. INTRODUCTION

Anthropogenic emission of carbon dioxide from the combustion of fossil fuels is the main contributor to global warming and climate changes. Carbon capture and sequestration (CCS) has been proposed to reduce CO_2 emissions. The major barrier for the implementation of CCS is that the CO_2 capture process is very expensive, which accounts for over 75% of the overall CCS costs [1]. Therefore, extensive studies have been conducted on the development of cost-effective and efficient CO_2 capture technologies, and calcium looping process is one of the most promising methods that could potentially achieve near zero CO_2 emission with a low cost [2-4].

Calcium looping utilizes the reversible reaction of calcium oxide and carbon dioxide for CO_2 capture, i.e. carbonation for CO_2 capture and calcination for sorbent regeneration. In recent years, good progresses have been made towards the commercialization of this technology. Several pilot plant trials have been initiated across the world and reported to operate in steady state with good CO_2 capture efficiencies [5-9]. However, calcium looping still faces a challenge related to the highly endothermic regeneration of CaO-based sorbents, thus a large amount of energy should be supplied continuously to the calcination reactor. The supply of regeneration energy is normally achieved by oxy-fuel combustion which makes the system more complex and expensive. In order to simplify the system and reduce the overall cost, a Ca-Cu chemical looping process was proposed recently [10] on the basis of "unmixed combustion" concept [11]. In this process, the energy needed for $CaCO_3$ decomposition can be supplied by the exothermic reduction of CuO with a hydrocarbon fuel (e.g. methane, which is an exothermic reaction), while the other two steps: carbonation of CaO and oxidation of Cu are both exothermic. Thus, no external energy is needed. The process has the advantages of no pure oxygen needed, easier control and potentially lower cost, compared with a normal calcium looping process.

Some preliminary work has been done on the conceptual design of Ca-Cu chemical looping process and the development of Ca/Cu-based sorbents that could be potentially applied [12]. Compared with the sorbents used in the typical calcium looping process, the sorbents for the new process contain CuO as well. It was found that the presence of CuO could have a negative effect on the reactivity of CaO for

CO_2 absorption, due to the agglomeration of Cu/CuO under high temperature[13]. Though this negative effect could be minimized by adopting individual CuO pellets separated from CaO pellets [14], composite materials with two active phases are also attractive [15-19], because of easier control of the component ratio and better heat transfer within the particles, which is critical for the feasibility and effectiveness of the combined Ca-Cu chemical looping process.

Since the CuO reduction reaction is to supply energy for the endothermic decomposition of $CaCO_3$, it is important for reactions rates of the two reactions to be similar, in order for the calciner to achieve a smooth and continuous operation. Lots of work has been conducted on kinetics of these reactions, and a general review of the studies is presented in Table 1. Though these experimental data can not be directly applied to the calcination process in CaL-CLC, the knowledge is valuable for a better understanding of the intrinsic characteristics of the reactions. Therefore, in the following section, we provide a brief review of the experimental and modeling work on the reduction of CuO and decomposition of $CaCO_3$.

1.1. Decomposition of $CaCO_3$

The kinetics of $CaCO_3$ decomposition under zero partial pressure of CO_2 has been extensively studied and the literature data seem to be consistent. Though it is expected that CO_2 partial pressure has a negative effect on the decomposition of $CaCO_3$, there is no consensus on the relationship in the literature. Ingraham and Marier [20] found that the decrease in the rate of $CaCO_3$ decomposition with increasing CO_2 pressure is proportional to the difference between the equilibrium pressure and the back pressure, which was later used in the modeling work [21, 22]. Darroudi and Searcy [23] observed a parabolic relationship between the reaction rate and the CO_2 partial pressure when $P_{CO2}>10^{-2}P_{eq}$ (P_{CO2}: CO_2 partial pressure, P_{eq}: CO_2 equilibrium pressure), though it could be ignored when CO_2 partial pressure is out of the range. Later, this relationship was adopted by Hu and Scaroni [24] in the modeling of limestone calcination in a furnace. On the other hand, Khinast et al. [25] showed an exponential rather than a linear decrease in the decomposition rate of limestone with the increase of CO_2 partial pressure.

In principle, the rate-limiting process during $CaCO_3$ decomposition can be the chemical kinetics, heat transfer through the particle to the reaction interface, or mass transport of released CO_2 from the reaction interface through the porous particle. The latter two are greatly influenced by the size of particles. Borgwardt [26] proposed a model of $CaCO_3$ decomposition assuming that the reaction is kinetic-controlled in the particle size range of 1-90 μm. Martínez et al. [27] observed almost no effect of particle size on decomposition rate when limestone diameter was below 0.3 mm under the atmosphere of 0-50 vol. % CO_2 at 1093-1183 K and 1 atm, which agreed with the work of Ar and Doğu [28]. The experimental and modeling results from the work of García-Labiano et al. [29] showed that intra-particle mass transfer and chemical reaction were the major rate-limiting steps for decomposition at 1123 K when particle size was in the range of 0.4-2 mm. Interestingly, Cui et al. [30] reported a linear relationship between apparent activation energy and reciprocal of particle size in the range of 36-88 nm by the multiple heating rate iso-conversion method. Pore surface area was also considered by some investigators to be a factor for the decomposition of $CaCO_3$. Borgwardt [26] proposed a direct linear relationship of decomposition rate with the pore surface area of $CaCO_3$. Then this factor was used by many researchers, though with different kinds of expression [24, 31, 32]. For comparison, kinetic data of $CaCO_3$ decomposition tested with different materials, physical property, and testing conditions in the literature are summarized in Table 1.

1.2. Reduction of CuO

The reaction of CuO with a reducing gas can be treated as a non-catalytic gas-solid reaction, thus different models for gas-solid reaction could be used to obtain its kinetic parameters. The shrinking core model (SCM) was usually used to represent the reduction kinetics of supported-CuO [33, 34]. García-Labiano et al. [35] studied the reduction kinetics of low-loaded CuO supported on alumina with three reducing gases: CH_4, H_2, and CO. When fuel gas concentration ranged in 5-70 vol. %, complete reduction was observed to be always attained in less than one minute at 1073 K, and reaction orders were determined to be 0.4, 0.6, and 0.8 for CH_4, H_2, and CO, respectively. The latter work exhibited a negative effect of increasing total pressure from 1 to 5 atm on the reaction rate [36]. Chuang et al. [37]

investigated the reaction rate of co-precipitated CuO (82.5 wt. % on Al_2O_3) with CO by a laboratory-scale fluidized bed reactor. Reaction order was found to be close to 1 and the reduction was reported to proceed via a direct route from CuO to Cu under 973 K, but follow a two-step mechanism with Cu_2O as an intermediate when temperature was higher. The reaction with H_2 was reported to follow the similar two routes, but the transition temperature was determined to be around 1073 K [38]. Reduction kinetics of high-loaded CuO-based material was also tested in the form of pellets and much lower reaction rate was exhibited when compared to that of particles [39]. Additionally, the reduction properties of CuO physically mixed with other metallic oxides were tested by Moghtaderi and Song [40]. Through experimental and theoretical analyses, it was found that activation energy and reaction order of a given physically mixed binary metal oxide were the arithmetic means of those of the parent metal oxides.

In addition, García-Labiano et al. [41] developed a changing grain size model (CGSM) to predict the reduction/oxidation rate of CuO/Cu and the temperature profile inside the particles, assuming that the particle consists of a matrix of non-porous grains of the same size with a uniform distribution, and the grain changes following a shrinking core model during reaction. Monazam et al. [42] evaluated the reactivity of CuO/bentonite with methane by 10 different rate models, and Johnson-Mehl-Avrami (JMA) model was reported to result in the best fit of the experimental data. Furthermore, the nucleation and nuclei growth model can describe the kinetics of the reduction/oxidation of CuO/Cu [34, 43].

For a better design of Ca-Cu chemical looping process, research on kinetic matching of the key reactions as well as heat transfer characteristics during calcination is required. For this purpose, a $CaCO_3$ sample was selected and a composite of CuO/Al_2O_3 was synthesized. Then, the kinetics of $CaCO_3$ decomposition and CuO reduction with CH_4 as reducing gas were obtained under chemical-controlled regime using a standard thermogravimetric analyzer (TGA). After the intrinsic reaction rates had been determined using gas-solid reaction models, the matching of heat generation and consumption in the calciner was evaluated by a specifically developed pseudo-homogeneous model.

2. EXPERIMENTAL SECTION

2.1. Materials and Sample Preparation

Pure calcium carbonate (≥99%, Alfa Aesar) was sieved to be within particle size ≤0.1 mm and then used to measure the kinetic parameters for the decomposition reaction. The reaction rate of CuO reduction with methane was determined using a composite containing 75 wt. % of CuO supported on alumina, which was synthesized from copper (II) acetate (98.0-102.0%, Ajax Finechem) and commercial activated aluminium oxide (≥99%, Sigma-Aldrich) via a wet mixing method as described in our previous work [13, 46]. In order to minimize the potential chemical interaction between CuO and Al_2O_3, -alumina was first calcined in air at 1373 K for 2 h to form -alumina [47]. During the preparation of CuO/Al_2O_3, predetermined copper (II) acetate was dissolved in distilled water with heating at 353 K to promote the process. Then, a specific amount of calcined and sieved -alumina (particle size ≤0.1 mm) was added into the solution which was continuously stirred for 5 h. After the mixture was dried in an oven at 393 K for 15 h and subsequently calcined in air for 30 min at 773 K, copper (II) acetate was decomposed to metal oxide. The sample was ground and sieved to be smaller than 0.1 mm before it was subjected to the test of reaction kinetics.

2.2. Thermogravimetric Analysis

Determination of reaction kinetics was carried out in a Cahn thermogravimetric analyzer apparatus (TGA, model 121). For a typical test, 5 mg sample was loaded on a quartz pan which was suspended in a quartz tube. The total gas flow rate was maintained to be 100 ml/min and the flow of each gas was controlled by accurate digital mass flow controller. Note that a calcination stage at 1123 K was carried out in the TG analyzer to stabilize the materials and to ensure the components of calcium or copper existed in the form of $CaCO_3$ and CuO. The isothermal tests of the reaction kinetics involved the following stages: (1) heating from room temperature to 1123 K at a rate of 50 K/min in 100 ml/minCO_2 (when testing the decomposition of $CaCO_3$) or in 100 ml/min air (when testing the reduction of CuO), and then stabilizing the conditions for 30 min, (2) heating/cooling step from 1123 K to a target temperature at a rate of 20 K/min under the same gas atmosphere, and (3) isothermal decomposition of

$CaCO_3$ or reduction of CuO with CH_4 at the target temperature in a specified gas atmosphere. The target test conditions for $CaCO_3$ decomposition were at 1048-1173 K in 0-60 vol. % CO_2 balanced by N_2, and it varied at 1073-1173 K in 10-40 vol. % CH_4 to study the reduction kinetics of CuO with CH_4. The data on sample mass during experiments were monitored and conversions of $CaCO_3$ and CuO were calculated on the basis of mass change, assuming that mass change was only due to the decomposition of $CaCO_3$ or reduction of CuO with CH_4.

2.3. Materials Characterization

Several analytical techniques were applied to characterize the materials. The BET surface area was determined with N_2 adsorption/desorption isotherms obtained at approximately 77 K using a Micromeritics TriStar 3000 instrument after sample outgassing under vacuum for 18 h at 473 K. The Hg porosimetry method was used in this work for density measurement of the samples. The main properties of the samples used in the work were presented in Table 2.

Table 2. Main physical properties of the samples tested.

3. REACTION KINETICS

3.1. Effect of Sample Size on Reaction Rates

There are several resistances, such as external and internal heat and mass transfer, which could affect the gas-solid reaction rate. Thus, a number of measures were taken to minimize these effects and to ensure that the reactions took place under chemical-controlled conditions. The diffusion effect of gas in the pore network was minimized by sieving particles of the samples to be smaller than 0.1 mm, and the intraparticle diffusion effect of particle size in this range was proved by several experiments to be negligible [27, 33]. Interparticle diffusion effects were minimized by maintaining a relatively high gas flow rate at 100 ml/min (comparing to the amount of sample tested) and a very small clearance between the sample and the mouth of the quartz basket in the TGA [40, 48]. To avoid the resistance due to interparticle diffusion, preliminary tests varying sample mass in the basket were carried out, and the

results are shown in Figure 1. It can be seen that when sample size was below 8 mg, its effect on both rate of $CaCO_3$ decomposition and CuO reduction could be ignored. For the above reasons, determination of kinetic parameters for the decomposition of $CaCO_3$ and reduction of CuO with CH_4 was conducted with a sample mass of around 5 mg in the work, and it was assumed that both reactions are in chemical-controlled regime under the conditions tested.

Figure 1. Effect of sample mass on (a) decomposition of $CaCO_3$ at 1173 K in 60 vol. % CO_2 balanced by N_2, and (b) reduction of CuO at 1073 K in 20 vol. % CH_4 balanced by N_2.

3.2. Kinetics of $CaCO_3$ Decomposition

Decomposition of $CaCO_3$ has been extensively studied, and various kinetic models were proposed to describe the process [26, 28, 31]. In this work, the Eq. (1) proposed by Fang et al. [49], with its integrated form Eq. (2), was used due to its simplicity and a good fitting of the data over the range of temperatures and CO_2 concentrations tested.

$$\frac{dX_{dec}}{dt} = k_{dec} \cdot (1 - X_{dec})^{2/3} \cdot (C_{eq,CO2} - C_{CO2}) \quad (1)$$

$$f(X_{dec}) = 3\left[1 - (1 - X_{dec})^{1/3}\right] = k_{dec} \cdot (C_{eq,CO2} - C_{CO2}) \cdot t \quad (2)$$

where, $C_{eq,CO2}$ is the equilibrium CO_2 concentration, which is an important parameter that determines the driving force of $CaCO_3$ decomposition, and its value is given by Eq. (3) [49]. C_{CO2} is CO_2 concentration, which can be calculated by Eq. (4).

$$C_{eq,CO2} = \frac{1.462\times10^{11}}{T} \exp(-19130/T) \quad (3)$$

$$C_{CO2} = \frac{P_{CO2}}{RT} \quad (4)$$

To determine the kinetic parameters of $CaCO_3$ decomposition, a series of experiments were carried out by varying the calcination temperature from 1048 K to 1173 K and keeping the CO_2 concentration constant. Figure 2 shows the effect of calcination temperature on the reaction rate of calcium carbonate in a N_2 atmosphere. As expected, the decomposition rate increases with the rise of calcination

temperature. When calcination temperature was at 1048 K, it took approximately 240 s to reach 100% conversion. However, less than 50 s was sufficient for full conversion when calcination temperature was increased to 1173 K.

Figure 2. Effect of calcination temperature on $CaCO_3$ decomposition in N_2. Experimental results are represented by symbols, and kinetic model predictions are represented by lines.

By plotting curves of $3\left[1-(1-X_{dec})^{1/3}\right]$ verses time according to Eq. (2) for six calcination temperatures presented in Figure 2, the slopes representing the values of $k_{dec}(C_{eq,CO2}-C_{CO2})$ were determined. Then the plotting of $\ln(k_{dec})$ against the inverse of temperature according to Eq. (5) results in a straight line with a slope and an intercept, which are $-E_{dec}/R$ and the pre-exponential factor A_{dec}, respectively, as shown in Figure 3. Here, the value of pre-exponential factor (A_{dec}) and the activation energy (E_{dec}) for the decomposition of $CaCO_3$ was determined to be 47817 m^3/(mol s) and 157.5 kJ/mol, which is included in Table 2. The activation energy determined over the temperature range of 1048-1173 K in this work is in close agreement with the reported values of 154-170 kJ/mol in the literature [20, 29, 44], but is different from that in other studies [23, 26, 27]. The difference mainly derives from the inherent complexity of the calcination process, as the existence of impurities, the physical process such a sintering, and the operational conditions could all contribute to the variations [28, 44].

$$lnk_{dec} = lnA_{dec} + (-\frac{E_{dec}}{R}) \cdot \frac{1}{T} \quad (5)$$

Figure 3. Plot of $\ln(k_{dec})$ vs. 1/T to determine the kinetic parameters of $CaCO_3$ decomposition.

Though previous experimental data are sufficient to determine the kinetic parameters of $CaCO_3$ decomposition by Eq. (2), it is also necessary to verify the model by means of its prediction of the effect

of CO_2 partial pressure on the reaction rate. This was done by plotting the reaction curves for different CO_2 partial pressure in the range of 0-0.6 atm for a given temperature (1173 K) and total pressure (1 atm). Figure 4 shows that there is a dependence of the decomposition rate of calcium carbonate on the CO_2 partial pressure, and the increase of CO_2 partial pressure slows down the reaction process. Despite of the simplicity, there is a good agreement between the model predictions and all of the experimental data presented in the work, indicating that the model is able to simulate the calcination process of $CaCO_3$ in the range of conditions of interest for the CaL-CLC process with reasonable accuracy.

Figure 4. Effect of CO_2 partial pressure on $CaCO_3$ decomposition (at 1173 K and 1 atm). Experimental results are represented by symbols, and kinetic model predictions are represented by lines.

3.3. Kinetics of CuO Reduction with CH_4

Attempts were also made to fit our experimental data on reduction of CuO with CH_4 using rate expressions in the literature, and random nucleation model [34, 50] demonstrated the most satisfactory agreement with the measured results under the conditions tested. The differential and integral forms of the model are as follows,

$$\frac{dX_{red}}{dt} = k_{red} \cdot {C_{CH4}}^{n} \cdot (1 - X_{red}) \quad (6)$$

$$f(X_{red}) = -ln(1 - X_{red}) = k_{red} \cdot {C_{CH4}}^{n} \cdot t \quad (7)$$

$$C_{CH4} = \frac{P_{CH4}}{RT} \quad (8)$$

To study the kinetics of CuO reduction with CH_4, it is important to first determine the reaction order. Therefore, the effect of CH_4 concentration on the reaction rate of CuO was measured and the results were presented in Figure 5 using CH_4 partial pressure as the variable. It can be seen that the time to achieve complete conversion of CuO is very short even under the testing temperature of 1073 K. When the partial pressure of CH_4 was set to be 0.1 atm, approximately 60-70 s was enough for the full reduction of CuO, while only around 20-30 s was sufficient to complete the reaction when the partial

pressure of CH_4 was increased to be 0.4 atm. Once the experimental data of the influence of CH_4 partial pressure on the conversion of CuO reduction were obtained, it was possible to determine the reaction order following next procedure: 1) determining the values of ($k_{red}C_{CH4}^{n}$) by plotting the $-\ln(1-X_{red})$ curves verses time under different CH_4 partial pressure according to Eq. (7) and (8), and 2) plotting the logarithm of ($k_{red}C_{CH4}^{n}$) determined in step 1 against the logarithm of $C_{CH4,}$ according to Eq. (9). Then the slope obtained is the apparent reaction order (n) of the reduction of CuO with CH_4, as shown in Figure 6, and its value is 0.46, which is in reasonable agreement with the reported 0.4-0.5 in the literature [33, 35].

$$\ln[k_{red} \cdot {C_{CH4}}^{n}] = lnk_{red} + nlnC_{CH4} \quad (9)$$

Figure 5. Effect of CH_4 partial pressure on CuO reduction (at 1073 K). Experimental results are represented by symbols, and kinetic model predictions are represented by lines.

Figure 6. Plot of $\ln(k_{red}C_{CH4}^{n})$ vs. $\ln(C_{CH4})$ to determine the reaction order of CuO reduction with CH_4.

Kinetic parameters for the reduction of CuO with CH_4 were obtained by investigating the effect of temperature on the reaction rate, as shown in Figure 7. Through determining the slopes ($k_{red}C_{CH4}^{n}$) of $-\ln(1-X_{red})$ curves vs. time for the five temperatures according to Eq. (7), the values of the reaction rate constant (k) for different temperatures can be determined, since reaction order (n) has been obtained and CH_4 concentration was fixed at 2.17 mol/m^3 here, corresponding to 20 vol. % CH_4 at 1123 K. Then, the activation energy (E_{red}) and pre-exponential factor (A_{red}) were determined to be 79.2 kJ/mol and 482 $m^{1.38}/(mol^{0.46}\ s)$, respectively, according to Arrhenius expression of Eq. (5), as shown in Figure 8.

Figure 7. Effect of temperature on the curve of CuO reduction with fixed CH_4 concentration at 2.17 mol/m^3 balanced by N_2. Experimental results are represented by symbols, and kinetic model predictions are represented by lines.

Figure 8. Plot of ln(k_{red}) vs. 1/T to determine the kinetic parameters of CuO reduction with CH_4.

To demonstrate the accuracy of the model, the predicted results using the kinetic parameters determined as aforementioned were also shown in Figure 5 and 7. Though there are some variations between the experimental results with the model predictions, especially when temperature was close to 1173 K, these differences were in an acceptable range. Thus, the model with the determined kinetic data can be used to simulate the reduction process of CuO with CH_4 under conditions of interest for CaL-CLC. Moreover, it should be noted that it was found that the products (H_2O and CO_2) of CuO reduction with CH_4 have no effect on the reaction rate, but the experimental data was not presented here. This result is in agreement with the observations presented in the literature [33, 35].

4. REACTOR MODELLING AND DISCUSSION

4.1. Mathematical Modelling

A pseudo-homogeneous model [51-53] was used in this work to describe the progressive reduction of CuO with CH_4 and the decomposition of $CaCO_3$ in a packed bed, and the following assumptions were adopted in the simulation: an ideal plug flow pattern, adiabatic reactor wall, negligible intra-particle mass and temperature gradients, ideal gas behavior, a constant bed voidage, and a uniform particle size in the bed. Note that it is a dynamic model, as CuO and $CaCO_3$ were gradually converted into Cu and CaO during the running of the calciner in the CaL-CLC system.

In the dynamic model, rate expressions of CuO reduction with CH_4 and $CaCO_3$ decomposition obtained in the previous section were utilized, and their molar rates per unit volume of material were calculated by Eq. (10) and (11) respectively, where ρ_{CuO} and ρ_{CaCO3} are the molar density of CuO and $CaCO_3$.

$$r_{red} = \rho_{CuO} \frac{dX_{red}}{dt} \tag{10}$$

$$r_{dec} = \rho_{CaCO3} \frac{dX_{dec}}{dt} \quad (11)$$

In addition to the reaction models, mass and energy balances, and the pressure drop were employed in the simulation of the multi-component system. The mass balance in the fixed-bed was governed using the pseudo-homogeneous model as follows,

$$\varepsilon \frac{\partial C_i}{\partial t} + \frac{\partial (uC_i)}{\partial z} = (1-\varepsilon) r_i \quad (12)$$

where, ε is the bed voidage, C_i is the molar concentration of gas species i (CH_4, CO_2, and H_2O), u is the superficial velocity.

The pseudo-homogenous energy equation for an adiabatic fixed-bed reactor was expressed as Eq. (13).

$$\left[(1-\varepsilon)\rho_s c_{ps} + \varepsilon \rho_g c_{pg}\right] \frac{\partial T}{\partial t} = -\frac{\partial (u \rho_g c_{pg} T)}{\partial z} - (1-\varepsilon) r_{red} \Delta H_{red} - (1-\varepsilon) r_{dec} \Delta H_{dec} \quad (13)$$

where, ρ_s and c_{ps} are the average density and heat capacity of the solids in the reactor, ρ_g and c_{pg} are density and heat capacity of the gas mixture. ΔH_{red} and ΔH_{dec} represent the reaction heat of CuO reduction with CH_4 and that of $CaCO_3$ decomposition, respectively.

The pressure loss in the fixed-bed reactor was calculated using the Ergun equation as follows [54],

$$\frac{dP}{dz} = \frac{150(1-\varepsilon)^2 \mu u}{D_p^2 \varepsilon^3} + \frac{1.75(1-\varepsilon)\rho_g u^2}{D_p \varepsilon^3} \quad (14)$$

where, μ is the dynamic viscosity of the gas, and D_p is the equivalent diameter of pellets in the reactor.

The mathematical model was solved using the finite difference method in MATLAB, and the initial and boundary conditions are shown as Eq. (15) and (16).

$$C_i = C_{i,0} \quad T = T_{s,0} \quad P = 1\ atm \quad at\ t = 0 \quad (15)$$

$$C_i = C_{i,in} \quad T = T_{g,in} \quad P = 1\ atm \quad at\ z = 0 \quad (16)$$

Features of the fixed-bed reactor and the operating parameters used are summarized in Table 3, which were determined based on the preliminary conceptual design and the modeling work specifically for CaL-CLC in the literature [14, 51]. It should be noted that the theoretical $CuO/CaCO_3$ molar ratio used

for the combined Ca-Cu chemical looping process should be determined taking into account the type of reducing gas used, calcination temperature (reaction enthalpies), and the equilibrium pressure of CO_2 for the decomposition of $CaCO_3$. When CH_4 was used as reducing agent for the reduction of CuO, temperature of 1148 K and a $CuO/CaCO_3$ molar ratio of 3.2 were determined to be the theoretical condition for the simultaneous decomposition of $CaCO_3$ and reduction of CuO. Considering the conversion of CaO in carbonation stage is usually very low in cyclic operation, a great proportion of calcium exists in the form of CaO in addition to $CaCO_3$ at the beginning of calcination. In this work, we assume a maximum conversion of 30% during the carbonation, thus the material simulated has a Cu/Ca molar ratio of 0.96.

Table 3. Reactor characteristics and the operating parameters used in the case studied.

4.2. Analysis of Reactions in the Calciner

After developing the rate models of CuO reduction with CH_4 and $CaCO_3$ decomposition, it is possible to predict the temperature, gas concentration, and conversions profiles along the length of the reactor using the pseudo-homogeneous model as described abovve. Figure 9 shows the dynamic profiles of these parameters under the conditions that a gas stream containing 30 vol. % CH_4 and 70 vol. % CO_2 was fed into the reactor at 1148 K, and the initial solid temperature in the bed was set to 1148 K as well. Atmospheric pressure conditions were selected in this work as a low pressure is favorable to shift the equilibrium of $CaCO_3$ decomposition to form CO_2 [14]. It can be seen from Figure 9(c) that the concentration of CH_4 quickly decreased to zero when the feeding gas reached CuO, and a full conversion of CuO reduction was achieved, which is due to a very fast reduction rate of CuO reduction with CH_4 under the conditions studied. In contrast to the narrow reaction front of CuO reduction, the reaction zone of $CaCO_3$ decomposition is much wider. The fastest decomposition rate appeared just after the occurrence of CuO reduction. The reason is that CuO reduction released a large amount of heat and local temperature was largely raised, which was beneficial for $CaCO_3$ decomposition. Then

decomposition rate gradually decreased to a low level, and only approximately 90% of $CaCO_3$ was observed to convert into CaO at the end of calcination stage. Though the heat released from the exothermic reduction of CuO could be partially utilized through the endothermic decomposition of $CaCO_3$, the big difference in reaction rate between the two reactions could easily result in local overheating between two reaction fronts. As shown in Figure 9(b), the local temperature difference was around 90 K. Therefore, this area should be concerned as the hot spot, which could lead to activity loss of Cu/CuO and CaO in the next cycle of calcination, carbonation, and oxidation [14]. Furthermore, it is most likely that the problem of overheating in local area could be more severe if CuO and $CaCO_3$ are prepared in separate pellets compared to the condition that they are included in the same pellet where both reactions are taking place.

Figure 9. Dynamic profiles of (a) solid reaction conversion, (b) temperature, and concentration of (c) CH_4 and (d) CO_2 in an adiabatic fixed-bed calciner (inlet gas: 30 vol. % CH_4 and 70 vol. % CO_2, 1148 K).

Though CO_2 was observed to have no impact on the reduction process of CuO, its existence in the feeding gas could restrain the proceeding of $CaCO_3$ decomposition, thus it is important to investigate this influence on reactions and heat transfer in the calciner. Figure 10 shows the change of reaction conversions and temperature in the reactor outlet as a function of time, when CO_2 fraction in the reducing gas was varied in the range of 0-70 vol. %. Simulation results show that higher CO_2 fraction leads to longer breakthrough period because the feeding rate of CH_4 was reduced despite of the same amount of CH_4 needed for the reduction of CuO. This means that a longer time was needed for the reactor to be operated in the mode of calciner during the running of CaL-CLC process. Moreover, only a tiny impact of the decreased CH_4 concentration on the reduction rate of CuO was observed at the place where the reaction started, indicating that the reaction rate of CuO is sufficiently fast under the conditions studied. In contrast, decomposition rate of calcium carbonate was observed to decrease with

increasing the CO_2 fraction in feeding gas. When pure CH_4 was used as reducing gas, around 20 s is enough for the full decomposition of calcium carbonate. However, when 35 vol. % CO_2 was included in the feeding gas, the time needed to reach the same conversion was doubled. Further increasing the CO_2 fraction could lead to a very slow decomposition process, resulting in only partial $CaCO_3$ decomposition. On the basis of these results, it is concluded that higher CO_2 fraction in CH_4 could enlarge the mismatching in the reduction of CuO with CH_4 and the $CaCO_3$ decomposition.

Figure 10. Effect of CO_2 fractions in feeding gas on (a) reaction conversions and (b) temperature of the reactor outlet (inlet gas temperature: 1148 K).

The change of solid conversions and temperature in the calciner outlet of CaL-CLC is presented in Figure 11 for different fractions of steam in CH_4 when the process was carried out with inlet gas at 1148 K and 1 atm. The addition of steam to the reducing gas is mainly to reduce the partial pressure of CO_2 in the reaction atmosphere of the calciner, i.e. to accelerate the decomposition of $CaCO_3$. This arrangement is technically feasible, as steam could be easily condensed and separated from the off-gas from calciner, and then the high-concentration CO_2 stream could be used or permanently stored in geological formations. One alternative heat source for generating steam could be the high-temperature O_2-lean air from the outlet of the oxidator in CaL-CLC. As shown in Figure 11, the addition of steam could delay the occurrence of the reaction breakthrough. When pure CH_4 is used as reducing gas, the time to reach breakthrough at the calciner outlet is a little over 200 s. However, when 70 vol. % CH_4 in the reducing gas is replaced by steam, the duration to breakthrough is increased to be around 500 s. The delay of the occurrence of reaction breakthrough is similar to the observations when the same fraction of CO_2 was used in the feeding gas. However, in contrast to the inhibition of CO_2 on the decomposition of $CaCO_3$, it is advantageous to have steam as diluent gas in CH_4, as a much better kinetic matching between the CuO reduction and $CaCO_3$ decomposition was demonstrated, which could also be observed from the lower local temperature peak in Figure 11(b). Although adding steam into the feeding gas is possible to

decrease the operating temperature in the calciner, which could reduce the problems of CaO de-activation and Cu/CuO agglomeration, this adjustment should be made carefully. As shown in Figure 12 (the feeding gas temperature and initial solid temperature were set to be the same during simulation), the mismatching between the reduction of CuO with CH_4 and the decomposition of $CaCO_3$ enlarged as decreasing the operating temperature from 1148 K to 1098 K. Additionally, the problem of overheating was intensified. When simulated for 1148 K, the maximum local temperature difference in the calciner was around 60 K, which increased to be 100 K when the operating temperature was decreased to be 1098 K. This change is due to the different impact of the operating temperature on the reaction rate of $CaCO_3$ decomposition and CuO reduction.

Figure 11. Effect of steam fractions in CH_4 on (a) reaction conversions and (b) temperature of the reactor outlet (inlet gas temperature: 1148 K).

Figure 12. Effect of operating temperature on (a) reaction conversions and (b) temperature of the calciner outlet (inlet gas: 30 vol. % CH_4 and 70 vol. % H_2O).

5. CONCLUSIONS

Decomposition of $CaCO_3$ and reduction of CuO with CH_4 under the conditions of interest for the calcination stage in Ca-Cu chemical looping were investigated by TGA with a $CaCO_3$ powder and a synthesized CuO-based oxygen carrier. Kinetic parameters of the two reactions were determined experimentally, and subsequently incorporated into a dynamic model of an adiabatic fixed-bed reactor to simulate the calcination process in the CaL-CLC system. The model proposed is able to simulate profiles of solid conversions, gas concentrations, and temperature in the calciner. Local overheating is found in the calciner due to the different reaction rates of CuO reduction with CH_4 and the $CaCO_3$ decomposition. The addition of steam can reduce the level of overheating while the presence of high

concentration CO_2 can further enhance the overheating. It was also found that the operation temperature should be carefully chosen to minimize local overheating in the calciner.

NOMENCLATURE

C_{CH4}	CH_4 concentration, mol/m^3
C_{CO2}	CO_2 concentration, mol/m^3
$C_{eq,CO2}$	equilibrium concentration of CO_2, mol/m^3
C_i	concentration of gas 'i', mol/m^3
$C_{i,0}$	initial concentration of gas 'i', mol/m^3
$C_{i,in}$	concentration of gas 'i' in feeding gas, mol/m^3
c_{pg}	heat capacity of gas in the reator, J/(kg·K)
c_{ps}	heat capacity of solid in the reator, J/(kg·K)
D_p	particle diameter, m
k_{dec}	reaction rate constant of $CaCO_3$ decomposition, m^3/(mol·s)
k_{red}	reaction rate constant of CuO reduction, m$^{1.3875}$/(mol$^{0.4625}$·s)
n	reaction order, dimensionless
ΔH_{red}	heat of CuO reduction, J/mol
ΔH_{dec}	heat of $CaCO_3$ decomposition, J/mol
P	total pressure, Pa
P_{CO2}	CO_2 partial pressure, Pa
r_{red}	rate of CuO reduction, mol/(m^3·s)
r_{dec}	rate of the decomposition of $CaCO_3$, mol/(m^3·s)
r_i	formation/consumption rate of gas 'i', mol/(m^3·s)
R	ideal gas constant, J/(mol·K)

t	time, s
T	temperature, K
$T_{s,0}$	initial solid temperature in the reactor, K
$T_{g,in}$	temperature of the feeding gas, K
u	superficial velocity, m/s
X_{red}	conversion of CuO reduction, dimensionless
X_{dec}	conversion of $CaCO_3$ decomposition, dimensionless
z	axial coordinate in the reactor, m

Greek symbols

ε	bed voidage, dimensionless
ρ_{CuO}	molar density of CuO, mol/m^3
ρ_{CaCO3}	molar density of $CaCO_3$, mol/m^3
ρ_g	density of gas in the reactor, kg/m^3
ρ_s	density of solid in the reactor, kg/m^3
μ	dynamic viscosity of gas, kg/(m·s)

ACKNOWLEDGEMENT

This research was supported by the Fundamental Research Funds for the Central Universities (No. 0903005203225). Changlei Qin also acknowledges the Graduate School International Travel Award (GSITA) from The University of Queensland.

REFERENCES

[1] P.H.M. Feron, C.A. Hendriks, CO_2 Capture Process Principles and Costs, Oil Gas Sci. Technol., 60 (2005) 451-459.

[2] G. Curran, C. Rice, E. Gorin, Carbon Dioxide Acceptor Gasification Process, BCURA MM. Bull, 29 (1965) 1752.

[3] C. Han, D.P. Harrison, Simultaneous shift reaction and carbon dioxide separation for the direct production of hydrogen, Chem. Eng. Sci., 49 (1994) 5875-5883.

[4] T. Shimizu, T. Hirama, H. Hosoda, K. Kitano, M. Inagaki, K. Tejima, A Twin Fluid-Bed Reactor for Removal of CO_2 from Combustion Processes, Chem. Eng. Res. Des., 77 (1999) 62-68.

[5] S. Koppatz, C. Pfeifer, R. Rauch, H. Hofbauer, T. Marquard-Moellenstedt, M. Specht, H_2 Rich Product Gas by Steam Gasification of Biomass with In Situ CO_2 Absorption in a Dual Fluidized Bed System of 8 MW Fuel Input, Fuel Process. Technol., 90 (2009) 914-921.

[6] A. Charitos, N. Rodríguez, C. Hawthorne, M. Alonso, M. Zieba, B. Arias, G. Kopanakis, G. Scheffknecht, J.C. Abanades, Experimental Validation of the Calcium Looping CO_2 Capture Process with Two Circulating Fluidized Bed Carbonator Reactors, Ind. Eng. Chem. Res., 50 (2011) 9685-9695.

[7] R.W. Hughes, D.Y. Lu, E.J. Anthony, A. Macchi, Design, Process Simulation and Construction of An Atmospheric Dual Fluidized Bed Combustion System for In Situ CO_2 Capture Using High-Temperature Sorbents, Fuel Process. Technol., 86 (2005) 1523-1531.

[8] J. Ströhle, M. Junk, J. Kremer, A. Galloy, B. Epple, Carbonate looping experiments in a 1 MWth pilot plant and model validation, Fuel, 127 (2014) 13-22.

[9] B. Arias, M.E. Diego, J.C. Abanades, M. Lorenzo, L. Diaz, D. Martínez, J. Alvarez, A. Sánchez-Biezma, Demonstration of steady state CO_2 capture in a 1.7 MWth calcium looping pilot, Int. J. Greenhouse Gas Control, 18 (2013) 237-245.

[10] J.C. Abanades, R. Murillo, J.R. Fernandez, G. Grasa, I. Martínez, New CO_2 Capture Process for Hydrogen Production Combining Ca and Cu Chemical Loops, Environ. Sci. Technol., 44 (2010) 6901-6904.

[11] R.K. Lyon, J.A. Cole, Unmixed combustion: an alternative to fire, Combust. Flame, 121 (2000) 249-261.

[12] I. Martínez, M.C. Romano, J.R. Fernández, P. Chiesa, R. Murillo, J.C. Abanades, Process design of a hydrogen production plant from natural gas with CO2 capture based on a novel Ca/Cu chemical loop, Applied Energy, 114 (2014) 192-208.

[13] C. Qin, J. Yin, W. Liu, H. An, B. Feng, Behavior of CaO/CuO Based Composite in a Combined Calcium and Copper Chemical Looping Process, Ind. Eng. Chem. Res., 51 (2012) 12274-12281.

[14] J.R. Fernández, J.C. Abanades, R. Murillo, G. Grasa, Conceptual design of a hydrogen production process from natural gas with CO_2 capture using a Ca–Cu chemical loop, Int. J. Greenhouse Gas Control, 6 (2012) 126-141.

[15] V. Manovic, E.J. Anthony, Integration of calcium and chemical looping combustion using composite CaO/CuO-based materials, Environ Sci Technol, 45 (2011) 10750-10756.

[16] V. Manovic, E.J. Anthony, CaO-Based Pellets with Oxygen Carriers and Catalysts, Energy Fuels, 25 (2011) 4846-4853.

[17] V. Manovic, Y. Wu, I. He, E.J. Anthony, Core-in-Shell CaO/CuO-Based Composite for CO_2 Capture, Ind. Eng. Chem. Res., 50 (2011) 12384-12391.

[18] A. Kierzkoska, C.R. Müller, Development of calcium-based, copper-functionalised CO_2 sorbents to integrate chemical looping combustion into calcium looping, Energy Environ. Sci., 5 (2012) 6061-6065.

[19] C. Qin, J. Yin, C. Luo, H. An, W. Liu, B. Feng, Enhancing the performance of CaO/CuO based composite for CO_2 capture in a combined Ca–Cu chemical looping process, Chem. Eng. J., 228 (2013) 75-86.

[20] T.R. Ingraham, P. Marier, Kinetic studies on the thermal decomposition of calcium carbonate, Can. J. Chem. Eng., 41 (1963) 170-173.

[21] H. Mikulčić, E. von Berg, M. Vujanović, P. Priesching, L. Perković, R. Tatschl, N. Duić, Numerical modelling of calcination reaction mechanism for cement production, Chem. Eng. Sci., 69 (2012) 607-615.

[22] G.D. Silcox, J.C. Kramlich, D.W. Pershing, A mathematical model for the flash calcination of dispersed calcium carbonate and calcium hydroxide particles, Ind. Eng. Chem. Res., 28 (1989) 155-160.

[23] T. Darroudi, A.W. Searcy, Effect of carbon dioxide pressure on the rate of decomposition of calcite ($CaCO_3$), J. Phys. Chem., 85 (1981) 3971-3974.

[24] N. Hu, A.W. Scaroni, Calcination of pulverized limestone particles under furnace injection conditions, Fuel, 75 (1996) 177-186.

[25] J. Khinast, G.F. Krammer, C. Brunner, G. Staudinger, Decomposition of limestone: The influence of CO_2 and particle size on the reaction rate, Chem. Eng. Sci., 51 (1996) 623-634.

[26] R.H. Borgwardt, Calcination kinetics and surface area of dispersed limestone particles, AICHE J., 31 (1985) 103-111.

[27] I. Martínez, G. Grasa, R. Murillo, B. Arias, J.C. Abanades, Kinetics of Calcination of Partially Carbonated Particles in a Ca-Looping System for CO_2 Capture, Energy Fuels, 26 (2012) 1432-1440.

[28] İ. Ar, G. Doğu, Calcination kinetics of high purity limestones, Chem. Eng. J., 83 (2001) 131-137.

[29] F. García-Labiano, A. Abad, L.F. de Diego, P. Gayán, J. Adánez, Calcination of calcium-based sorbents at pressure in a broad range of CO_2 concentrations, Chem. Eng. Sci., 57 (2002) 2381-2393.

[30] Z. Cui, Y. Xue, L. Xiao, T. Wang, Effect of Particle Size on Activation Energy for Thermal Decomposition of Nano-$CaCO_3$, Journal of Computational and Theoretical Nanoscience, 10 (2013) 569-572.

[31] Y. Zheng, C. Zheng, Z. Liu, X. Shi, Modelling for Flash Calcination and Surface Area Development of Dispersed Limestone Particles, Developments in Chemical Engineering and Mineral Processing, 8 (2000) 233-243.

[32] G. Marbán, A.B. Fuertes, A Simple Method for Studying the Kinectics of Gas-solid Reactions in a Fludized Bed Reactor, Chem. Eng. Commun., 130 (1994) 241-250.

[33] A. Abad, J. Adánez, F. García-Labiano, L.F. de Diego, P. Gayán, Modeling of the chemical-looping combustion of methane using a Cu-based oxygen-carrier, Combust. Flame, 157 (2010) 602-615.

[34] J. Adanez, A. Abad, F. Garcia-Labiano, P. Gayan, L.F. de Diego, Progress in Chemical-Looping Combustion and Reforming technologies, Prog. Energy Combust. Sci., 38 (2012) 215-282.

[35] F. García-Labiano, L.F. de Diego, J. Adánez, A. Abad, P. Gayán, Reduction and Oxidation Kinetics of a Copper-Based Oxygen Carrier Prepared by Impregnation for Chemical-Looping Combustion, Ind. Eng. Chem. Res., 43 (2004) 8168-8177.

[36] F. García-Labiano, J. Adánez, L.F. de Diego, P. Gayán, A. Abad, Effect of Pressure on the Behavior of Copper-, Iron-, and Nickel-Based Oxygen Carriers for Chemical-Looping Combustion, Energy Fuels, 20 (2005) 26-33.

[37] S.Y. Chuang, J.S. Dennis, A.N. Hayhurst, S.A. Scott, Kinetics of the chemical looping oxidation of CO by a co-precipitated mixture of CuO and Al_2O_3, Proceedings of the Combustion Institute, 32 (2009) 2633-2640.

[38] S.Y. Chuang, J.S. Dennis, A.N. Hayhurst, S.A. Scott, Kinetics of the chemical looping oxidation of H_2 by a co-precipitated mixture of CuO and Al_2O_3, Chem. Eng. Res. Des., 89 (2011) 1511-1523.

[39] A.L. García-Lario, I. Martínez, R. Murillo, G. Grasa, J.R. Fernández, J.C. Abanades, Reduction Kinetics of a High Load Cu-based Pellet Suitable for Ca/Cu Chemical Loops, Ind. Eng. Chem. Res., 52 (2013) 1481-1490.

[40] B. Moghtaderi, H. Song, Reduction Properties of Physically Mixed Metallic Oxide Oxygen Carriers in Chemical Looping Combustion, Energy Fuels, 24 (2010) 5359-5368.

[41] F. García-Labiano, L.F. de Diego, J. Adánez, A. Abad, P. Gayán, Temperature variations in the oxygen carrier particles during their reduction and oxidation in a chemical-looping combustion system, Chem. Eng. Sci., 60 (2005) 851-862.

[42] E.R. Monazam, R. Siriwardane, R.W. Breault, H.J. Tian, L.J. Shadle, G. Richards, S. Carpenter, Kinetics of the Reduction of CuO/Bentonite by Methane (CH_4) during Chemical Looping Combustion, Energy Fuels, 26 (2012) 2779-2785.

[43] M.M. Hossain, H.I. de Lasa, Chemical-looping combustion (CLC) for inherent CO_2 separations--a review, Chem. Eng. Sci., 63 (2008) 4433-4451.

[44] J.-T. Lee, T.C. Keener, M. Knoderer, S.-J. Khang, Thermal decomposition of limestone in a large scale thermogravimetric analyzer, Thermochim. Acta, 213 (1993) 223-240.

[45] Juan Adánez, Francisco García-Labiano, Luis F. de Diego, Ainhoa Plata, Javier Celaya, Pilar Gayán, A. Abad, Optimizing the Fuel Reactor for Chemical Looping Combustion, in: 17th International Conference on Fluidized Bed Combustion, Jacksonville, Florida, USA, 2003, pp. 173-182.

[46] C. Qin, W. Liu, H. An, J. Yin, B. Feng, Fabrication of CaO-Based Sorbents for CO_2 Capture by a Mixing Method, Environ. Sci. Technol., 46 (2012) 1932-1939.

[47] H. Lu, A. Khan, S.E. Pratsinis, P.G. Smirniotis, Flame-Made Durable Doped-CaO Nanosorbents for CO_2 Capture, Energy Fuels, 23 (2008) 1093-1100.

[48] C. Luo, Y. Zheng, J. Yin, C. Qin, N. Ding, C. Zheng, B. Feng, Effect of Sulfation during Oxy-Fuel Calcination Stage in Calcium Looping on CO_2 Capture Performance of CaO-Based Sorbents, Energy Fuels, 27 (2013) 1008-1014.

[49] F. Fang, Z.-S. Li, N.-S. Cai, Experiment and Modeling of CO_2 Capture from Flue Gases at High Temperature in a Fluidized Bed Reactor with Ca-Based Sorbents, Energy Fuels, 23 (2008) 207-216.

[50] M.M. Hossain, H.I. de Lasa, Reactivity and stability of Co-Ni/Al_2O_3 oxygen carrier in multicycle CLC, AICHE J., 53 (2007) 1817-1829.

[51] J.R. Fernández, J.C. Abanades, R. Murillo, Modeling of Cu oxidation in an adiabatic fixed-bed reactor with N_2 recycling, Applied Energy, 113 (2014) 1945-1951.

[52] J.R. Fernández, J.C. Abanades, R. Murillo, Modeling of Cu oxidation in adiabatic fixed-bed reactor with N_2 recycling in a Ca/Cu chemical loop, Chem. Eng. J., 232 (2013) 442-452.

[53] W. Wang, S. Ramkumar, S. Li, D. Wong, M. Iyer, B.B. Sakadjian, R.M. Statnick, L.S. Fan, Subpilot Demonstration of the Carbonation–Calcination Reaction (CCR) Process: High-Temperature CO_2 and Sulfur Capture from Coal-Fired Power Plants, Ind. Eng. Chem. Res., 49 (2010) 5094-5101.

[54] S. Ergun, Fluid flow through packed columns, Chem. Eng. Prog., 48 (1952) 89-94.

FIGURE CAPTIONS

Figure 1. Effect of sample mass on (a) decomposition of $CaCO_3$ at 1173 K in 60 vol. % CO_2 balanced by N_2, and (b) reduction of CuO at 1073 K in 20 vol. % CH_4 balanced by N_2.

Figure 2. Effect of calcination temperature on $CaCO_3$ decomposition in N_2. Experimental results are represented by symbols, and kinetic model predictions are represented by lines.

Figure 3. Plot of $\ln(k_{dec})$ vs. 1/T to determine the kinetic parameters of $CaCO_3$ decomposition.

Figure 4. Effect of CO_2 partial pressure on $CaCO_3$ decomposition (at 1173 K and 1 atm). Experimental results are represented by symbols, and kinetic model predictions are represented by lines.

Figure 5. Effect of CH_4 partial pressure on CuO reduction (at 1073 K). Experimental results are represented by symbols, and kinetic model predictions are represented by lines.

Figure 6. Plot of $\ln(k_{red}C_{CH4}^{n})$ vs. $\ln(C_{CH4})$ to determine the reaction order of CuO reduction with CH_4.

Figure 7. Effect of temperature on the curve of CuO reduction with fixed CH_4 concentration at 2.17 mol/m^3 balanced by N_2. Experimental results are represented by symbols, and kinetic model predictions are represented by lines.

Figure 8. Plot of $\ln(k_{red})$ vs. 1/T to determine the kinetic parameters of CuO reduction with CH_4.

Figure 9. Dynamic profiles of (a) solid reaction conversion, (b) temperature, and concentration of (c) CH_4 and (d) CO_2 in an adiabatic fixed-bed calciner (inlet gas: 30 vol. % CH_4 and 70 vol. % CO_2, 1148 K).

Figure 10. Effect of CO_2 fractions in feeding gas on (a) reaction conversions and (b) temperature of the reactor outlet (inlet gas temperature: 1148 K).

Figure 11. Effect of steam fractions in CH_4 on (a) reaction conversions and (b) temperature of the reactor outlet (inlet gas temperature: 1148 K).

Figure 12. Effect of operating temperature on (a) reaction conversions and (b) temperature of the calciner outlet (inlet gas: 30 vol. % CH_4 and 70 vol. % H_2O).

TABLES

Table 1. Some kinetic data determined for $CaCO_3$ decomposition and CuO reduction in the literature.

Reactions	Material	Physical structure	Experimental conditions	Kinetic model and parameter	Ref.
$CaCO_3$ decomposition	Limestone A (96.1 wt. % CaO)	Particle size: 0.075-0.8 mm Porosity: 0.044	TGA, T=1093-1183 K 0-50 vol. % CO_2	Grain model E=112.4 kJ/mol	[27]
	Limestone B (93.8 wt. % CaO)	Particle size: 0.075-0.125 mm Porosity: 0.020	TGA, T=1093-1183 K 0-50 vol. % CO_2	Grain model E=91.7 kJ/mol	
	Limestone (97.1 wt. % $CaCO_3$)	Particle size: 0.4-2 mm Porosity: 0.03	TGA, T=1048-1173 K 0-80 vol. % CO_2	Shrinking core model E=166 kJ/mol	[29]
	Limestone (95.8 wt. % $CaCO_3$)	Particle size: 0.4-2 mm Porosity: 0.3	TGA, T=1048-1173 K 0-80 vol. % CO_2	Changing grain size model E=131 kJ/mol	
	10 limestones:42.7-52.8 wt. % CaO	Particle size: 0.1-1.7 mm Porosity: 0.32-0.51	TGA, T=873-1173 K 0 vol. % CO_2	Shrinking core model E=156-213 kJ/mol	[28]
	Limestone (96.1 wt. % $CaCO_3$)	Particle size: 0.005-0.1 mm Porosity: 0.021-0.034	TGA, T=1053 K 0-6.5 vol. % CO_2	Modified random pore model	[25]
	Limestone (96-100 % purity)	Particle size: 2-7 mm	Large scale TGA, T= 973-1173 K 0-21 vol. % CO_2	Shrinking core model E=154-164 kJ/mol	[44]
	Two limestones (95% purity)	Particle size: 0.001-0.09 mm Porosity: 3%-8%	Differential reactor, T=789-1273 K 0 vol. % CO_2	E=205 kJ/mol	[26]
	Calcite	Slice 1-2 mm thick and 7 mm in diameter	Electrobalance, T=893-1073 K 0-100 vol. % CO_2	E=209 kJ/mol	[23]
	Precipitated $CaCO_3$ Calcite crystals	Particle size: <0.056 mm	T=1023-1173 K 0-100 vol. % CO_2	E=170 kJ/mol	[20]
CuO reduciton	10 wt. % CuO on alumina	Particle size: 0.1-0.3 mm Porosity: 0.57	TGA, T=723-1073 K 5-70 vol. % CH_4 5-70 vol. % H_2 5-70 vol. % CO	Shrinking core model n=0.4, E=60 kJ/mol n=0.6, E=33 kJ/mol n=0.8, E=14 kJ/mol	[35, 36]
	14 wt. % CuO on alumina	Particle size: 0.1-0.3 mm Porosity: 0.548	TGA, T=873-1073 K 5-70 vol. % CH_4	Shrinking core model n=0.5, E=106 kJ/mol	[33]
	60 wt. % CuO on alumina	Particle size: 0.2-0.4 mm Porosity: 0.2	TGA, T=923-1073 K 3-30 vol. % CH_4 3-40 vol. % H_2 5-50 vol. % CO	Shrinking core model n=0.9, E=74.5 kJ/mol n=1, E=23.3 kJ/mol n=1, E=25.5 kJ/mol	[39]
	60 wt. % CuO on SiO_2	Particle size: 1mm Porosity: 0.4	TGA, T=973-1123 K 100 vol. % CH_4	Shrinking core model n=1, E=41 kJ/mol	[45]
	60 wt. % CuO on bentonite	Particle size: 0.15-0.25 mm	TGA, T=1023-1173 K 20-100 vol. % CH_4	Johnson-Mehl-Avrami model n=1.55-2.16, E=37.3 kJ/mol	[42]
	82.5 wt. % CuO on alumina	Particle size: 0.355-0.5 mm Porosity: 0.75	Fludized bed, T=523-1173 K 1.1-9.77 vol. % CO	Shrinking core model n=1, E=52 kJ/mol	[37]
	62 wt. % CuO on alumina	Particle size: 0.09-0.106 mm	TGA, T=773-1073 K	Shrinking core model	[40]

	Porosity: 0.6	20-70 vol. % H_2	n=0.55, E=30kJ/mol	
		20-70 vol. % CO	n=0.8, E=16 kJ/mol	
82.5 wt. % CuO on alumina	Particle size: 0.355-0.5 mm	Fludized bed, T=723-1173 K	Shrinking core model	[38]
	Porosity: 0.75	2.6-10 vol. % H_2 ($CuO \rightarrow Cu_2O$)	n=1, E=58 kJ/mol	
		2.6-10 vol. % H_2 ($Cu_2O \rightarrow Cu$)	n=1, E=44 kJ/mol	

Table 2. Main physical properties of the samples tested.

Sample	$CaCO_3$	CuO/Al_2O_3
CaO (wt. %)	≥99	0
CuO (wt. %)	0	75
Al_2O_3 (wt. %)	0	25
BET surface area (m^2/kg)	6.6	3750.8
True density (kg/m^3)	2674.1	5427
Activation energy for decomposition/reduction (kJ/mol)	157.5	79.2

Table 3. Reactor characteristics and the operating parameters used in the case studied.

Parameters	Values
Reactor length (m)	7
Reactor diameter (m)	0.3
Reactors pellet diameter (m)	0.022
Bed voidage	0.5
Feed gas temperature (K)	1148
Initial solid temperature (K)	1148
Pressure (Pa)	101325
Superficial velocity (m/s)	2
Solid density (kg/m^3)	3602.5
Solid heat capacity (J/(kg K))	934.61

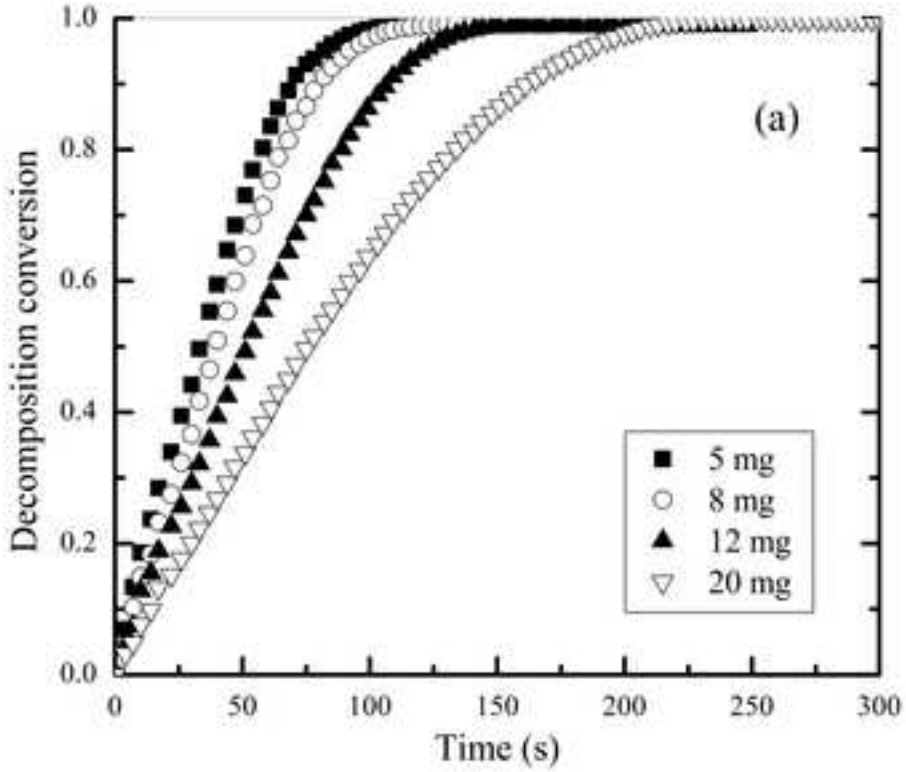

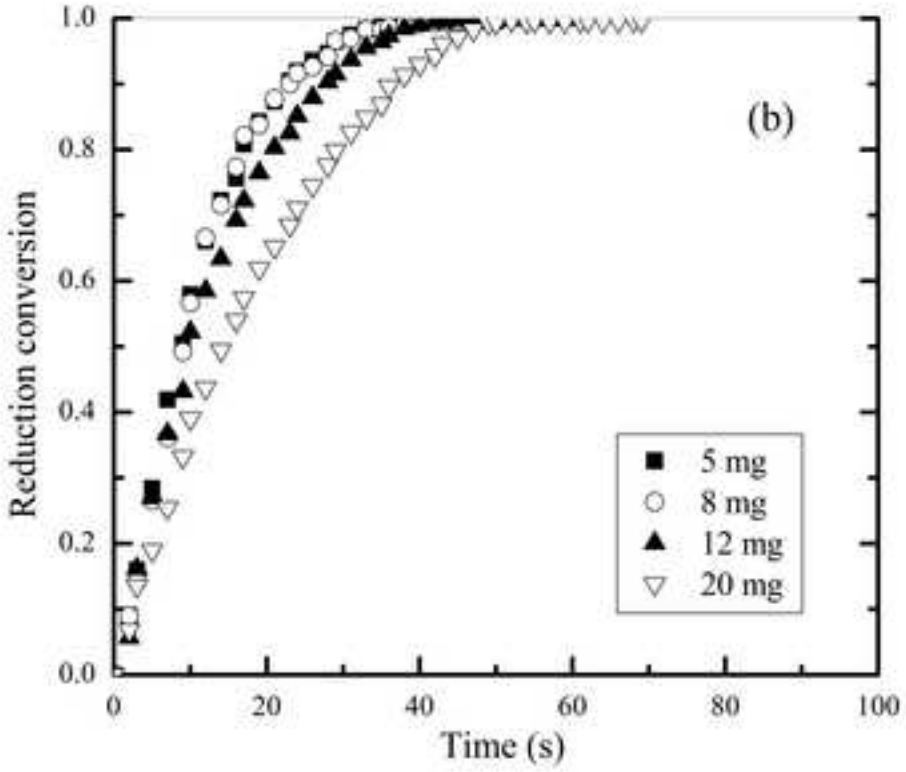

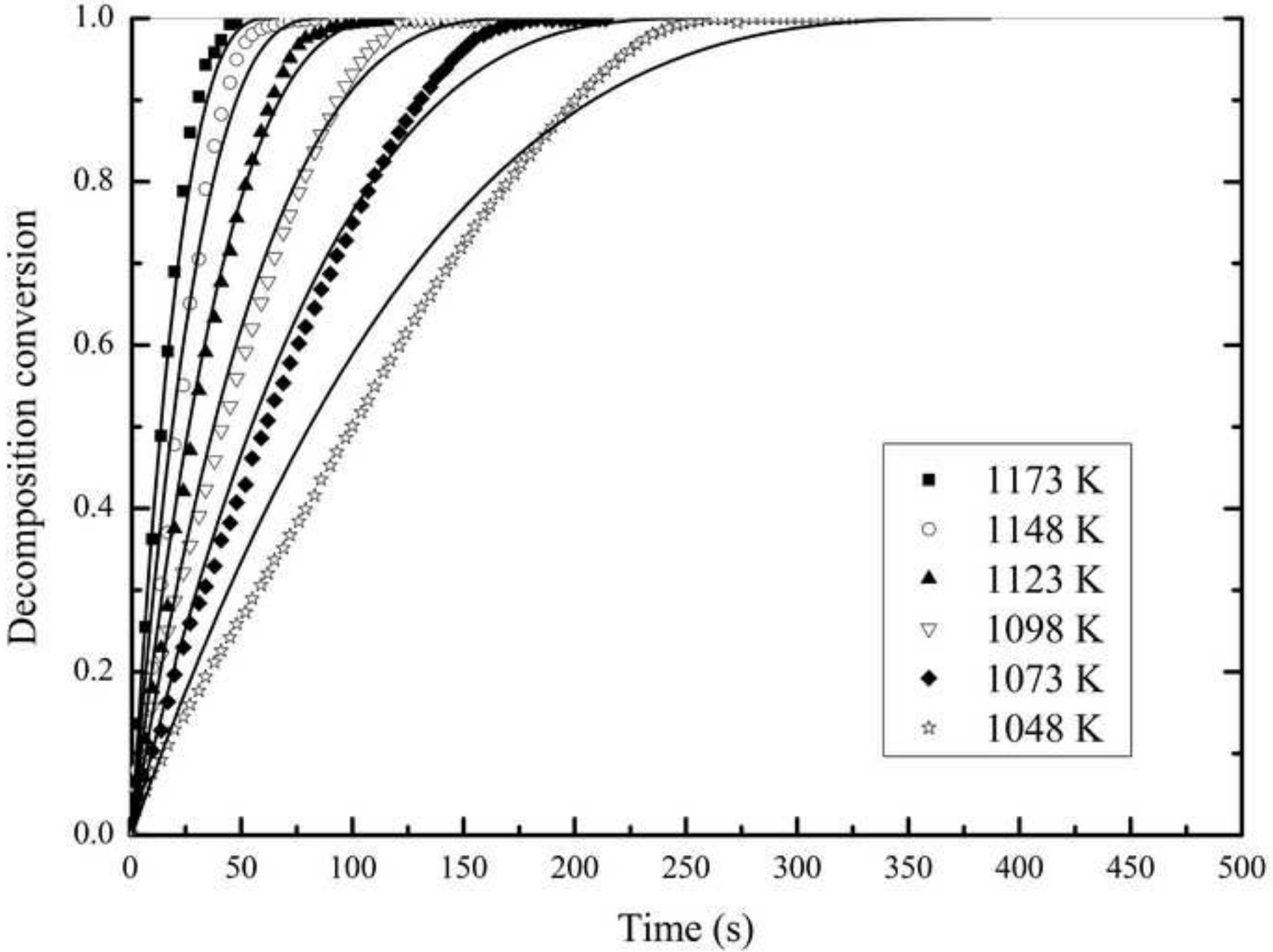

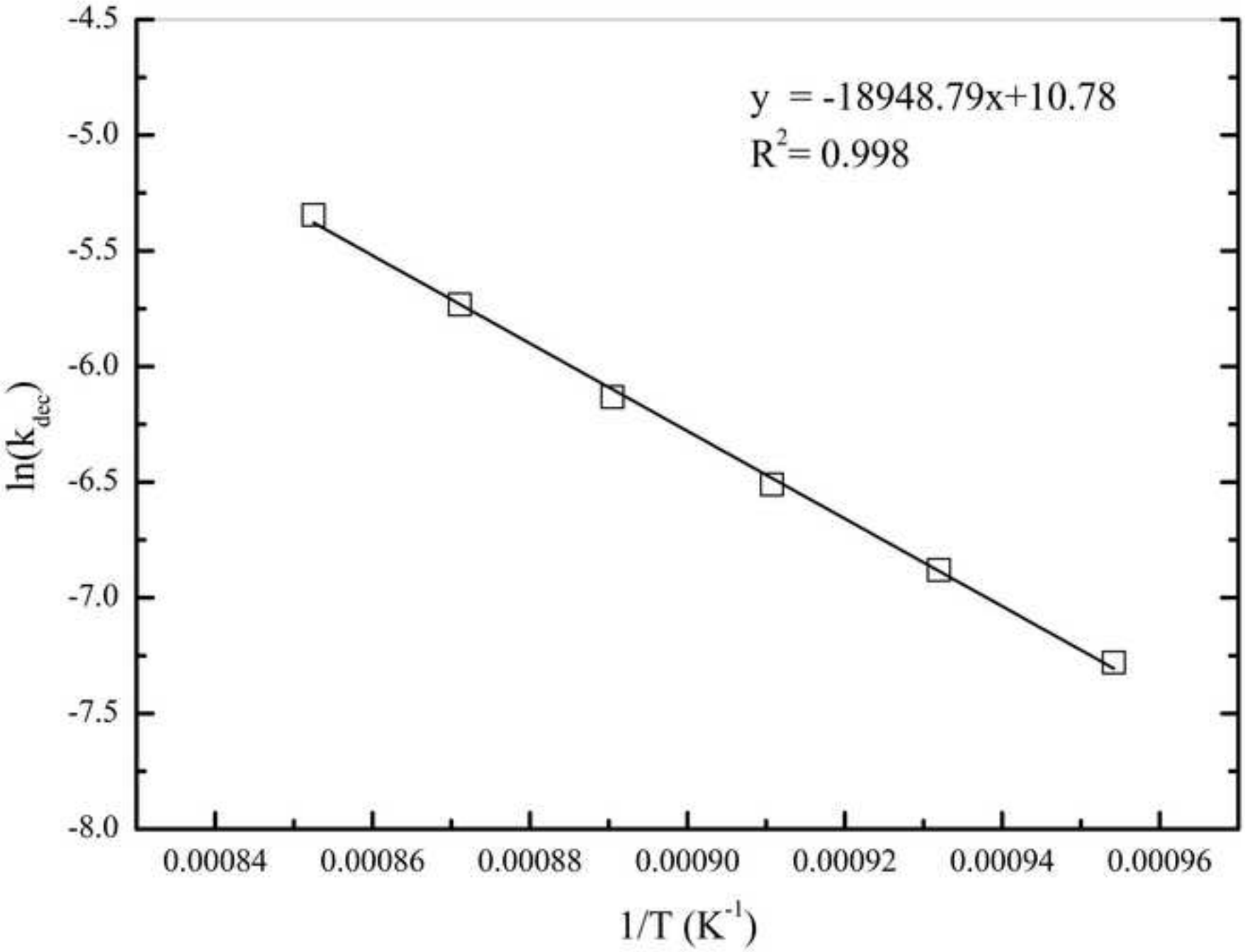

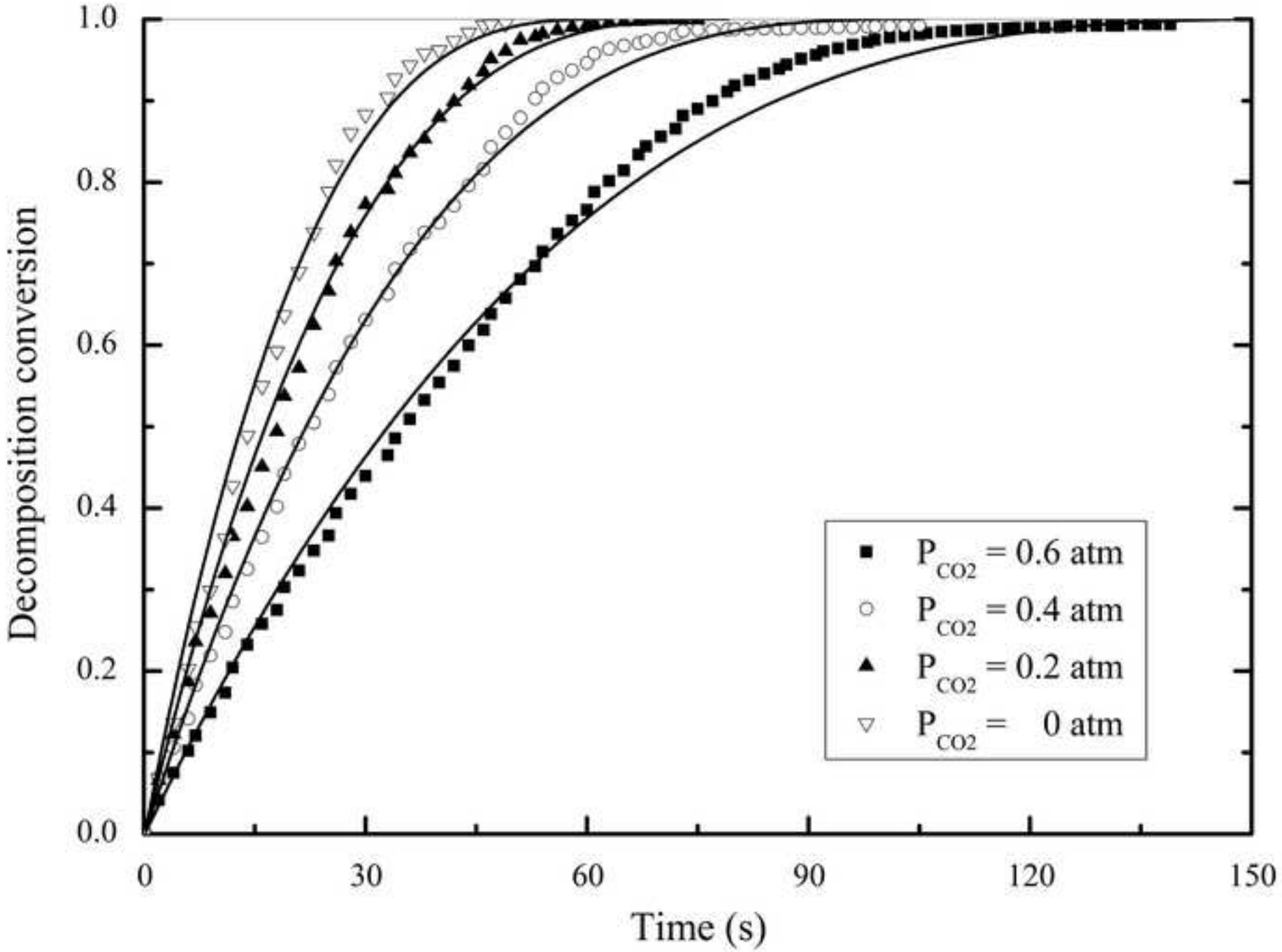

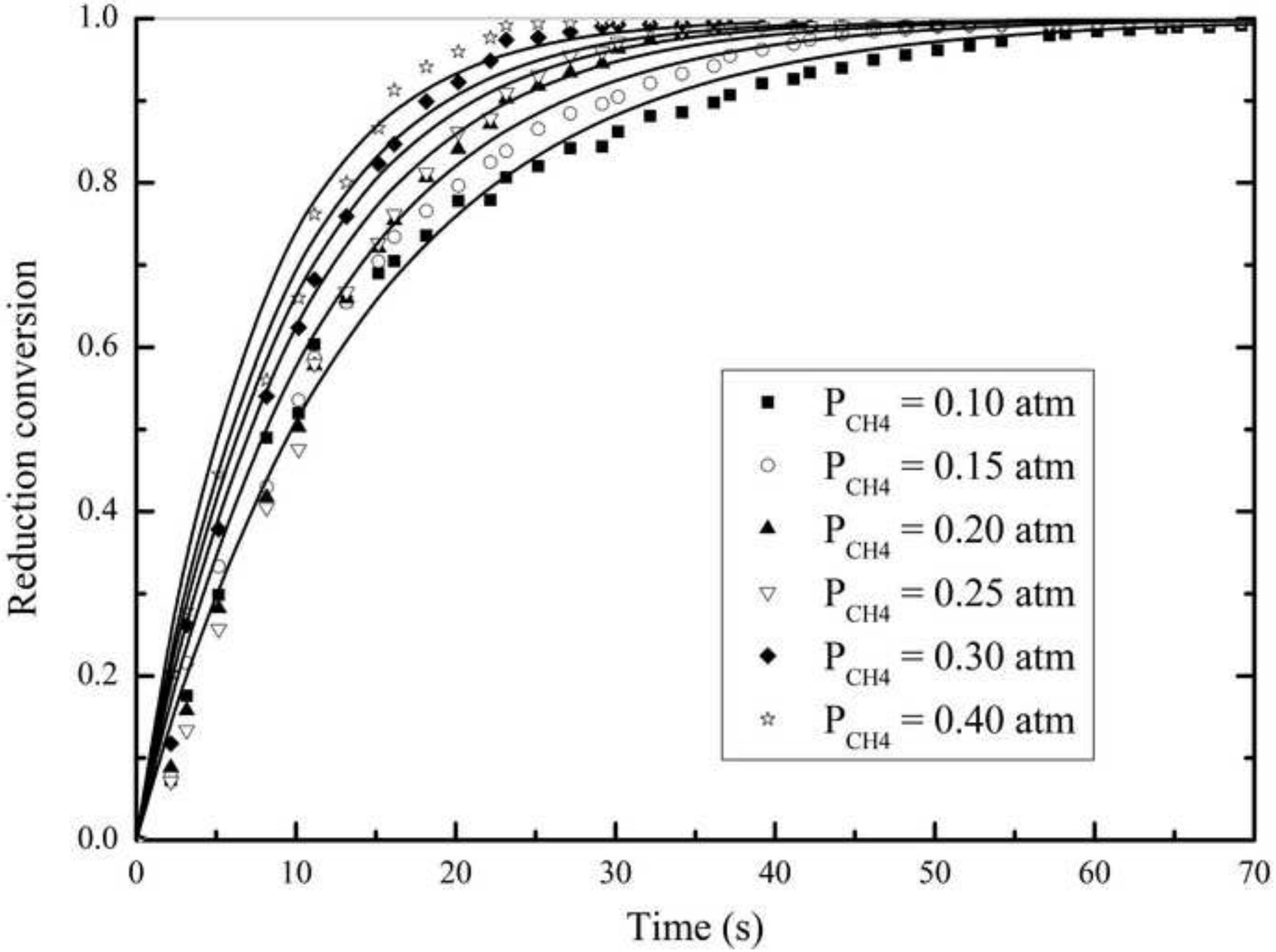

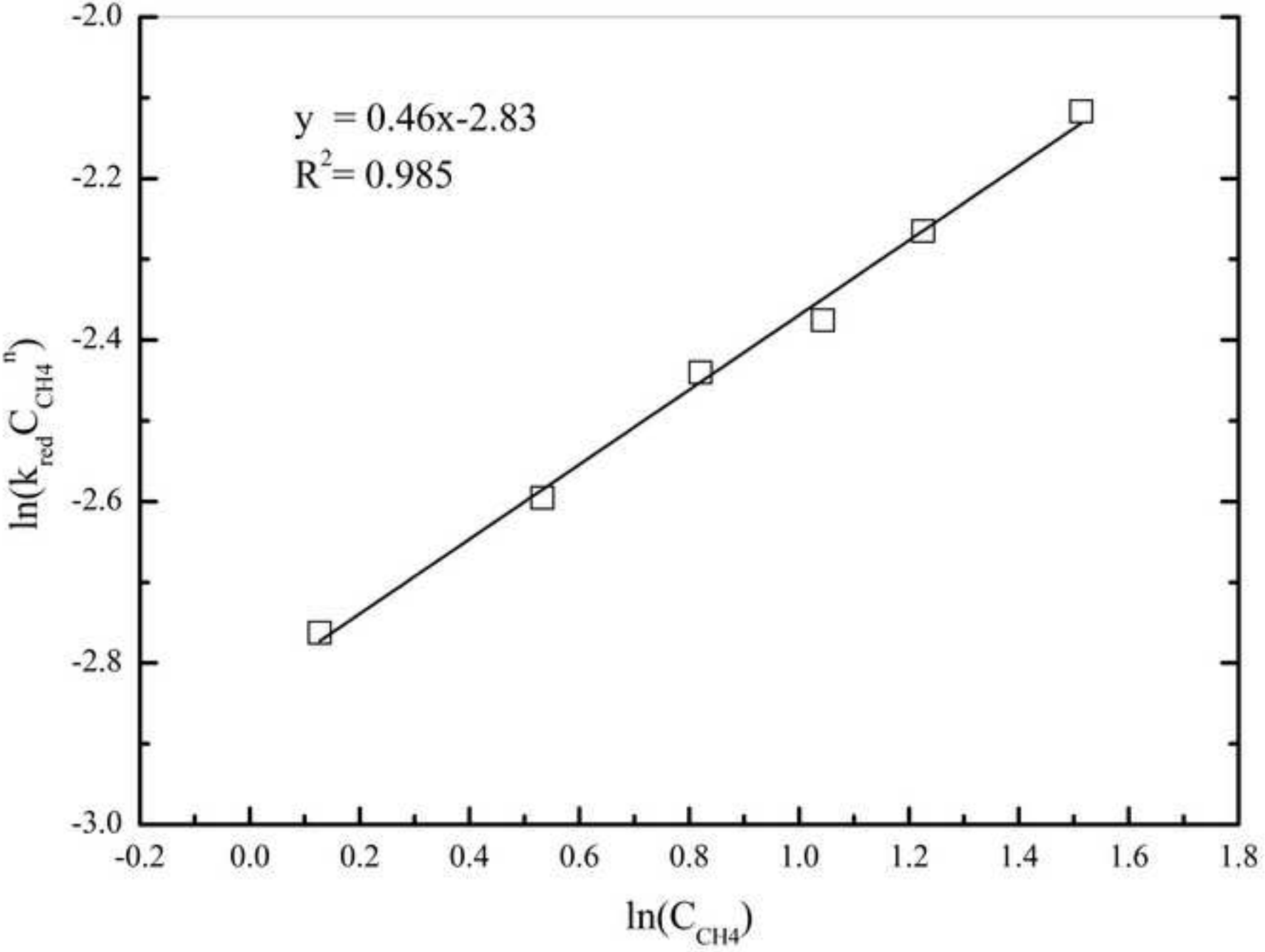

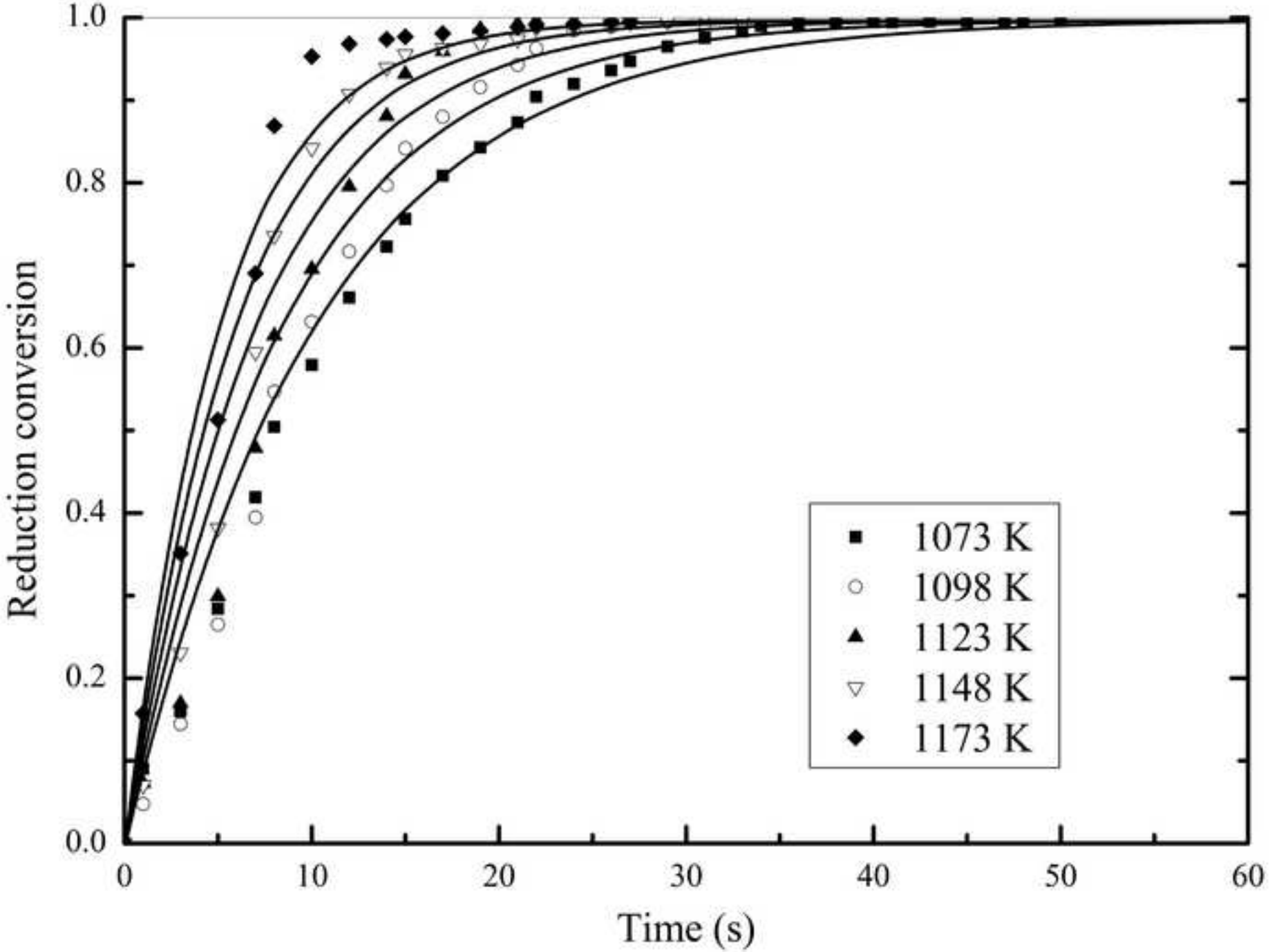

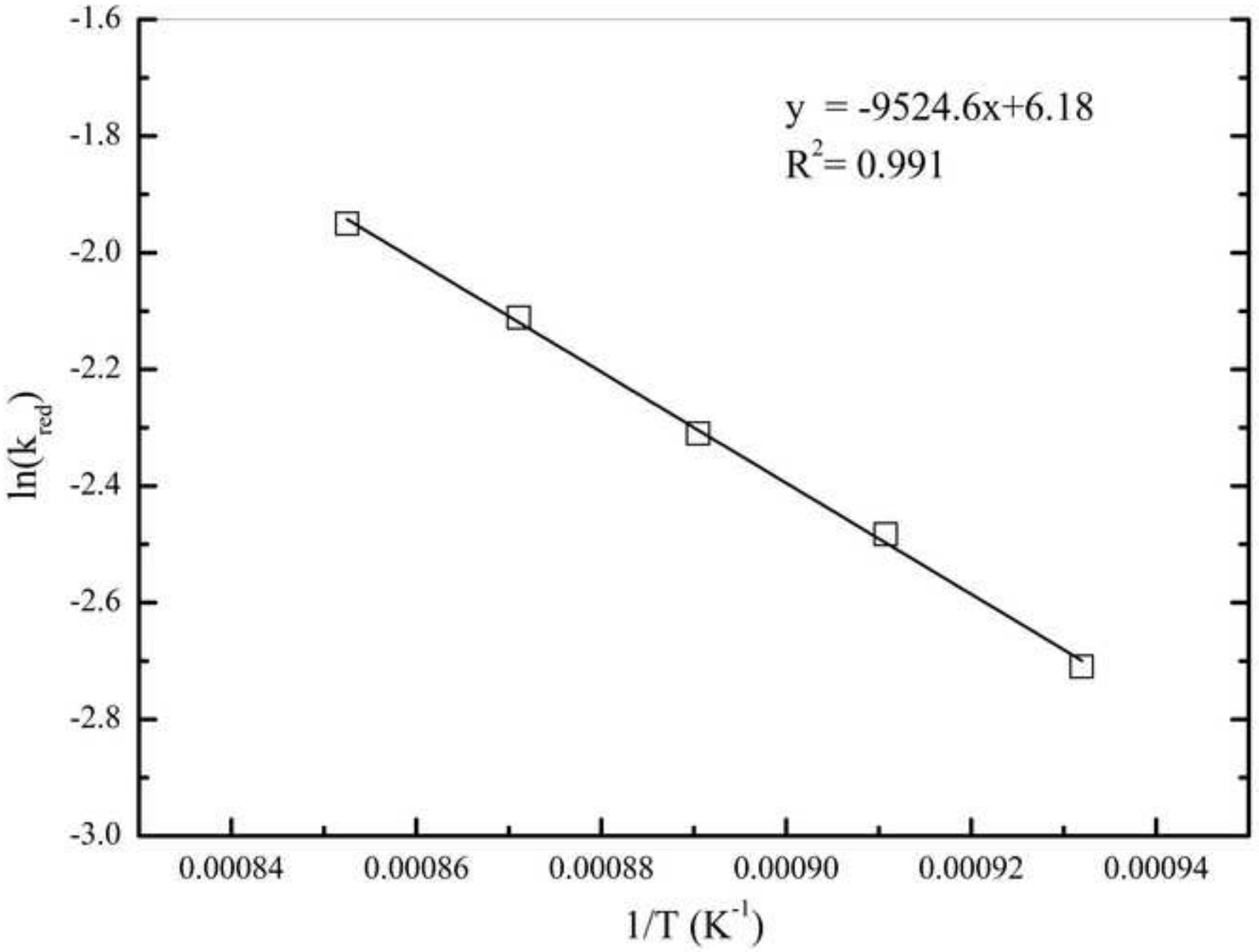

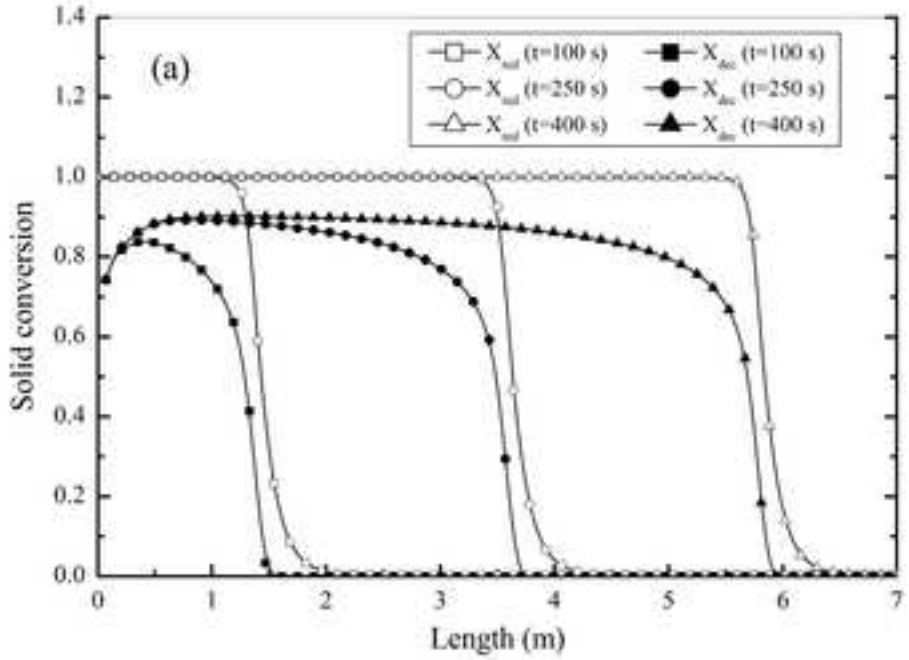

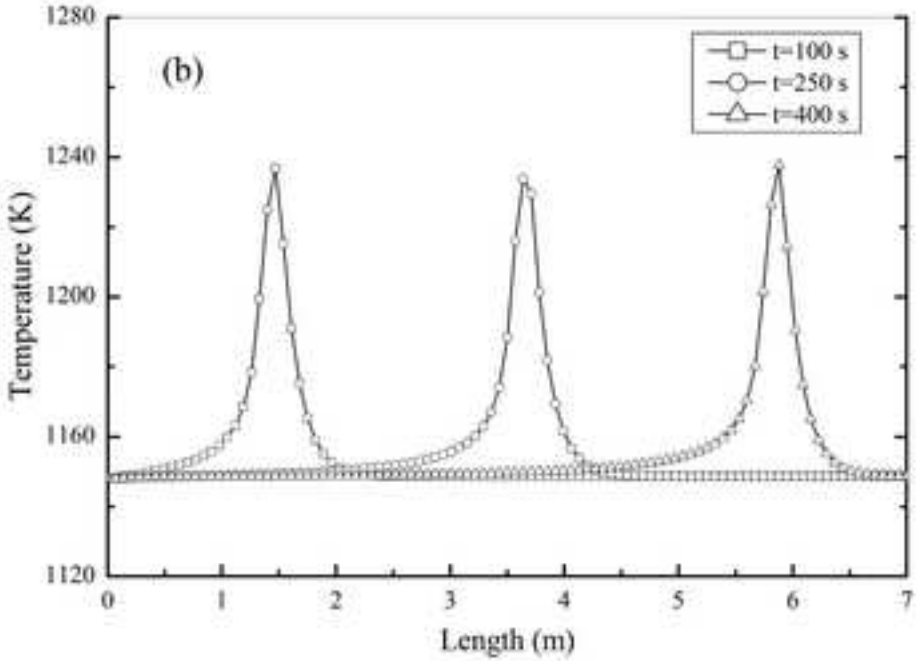

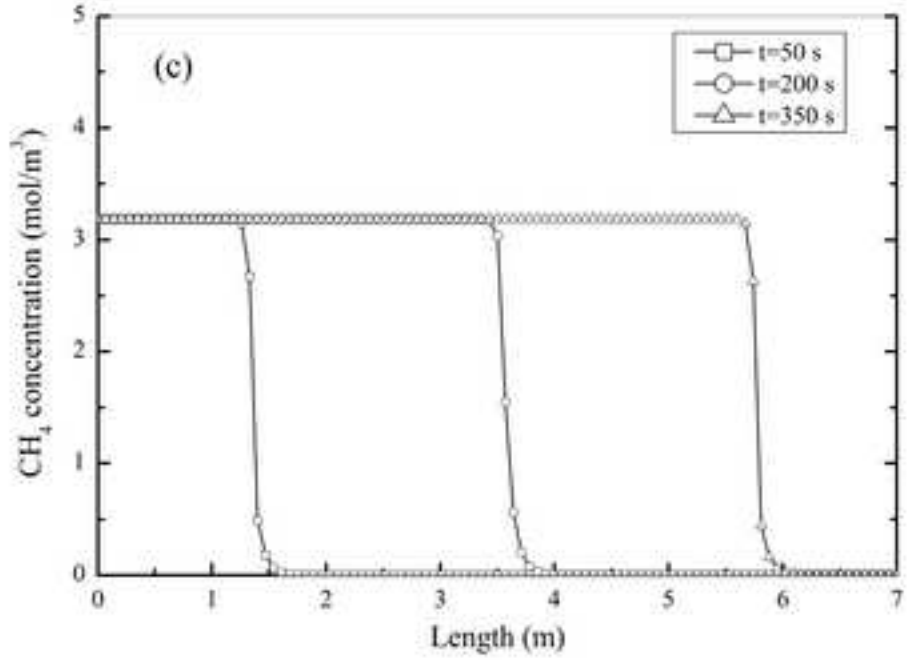

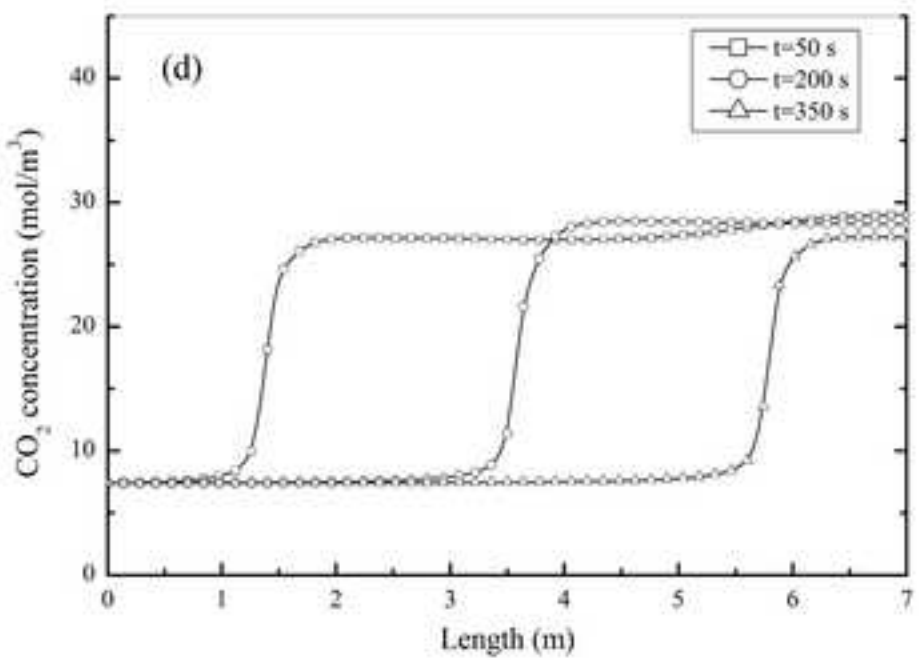

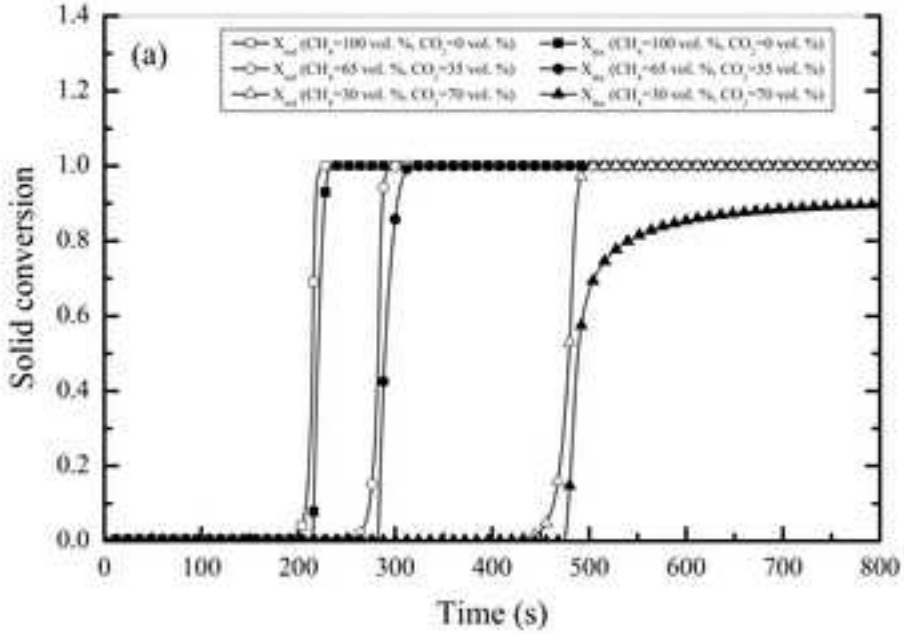

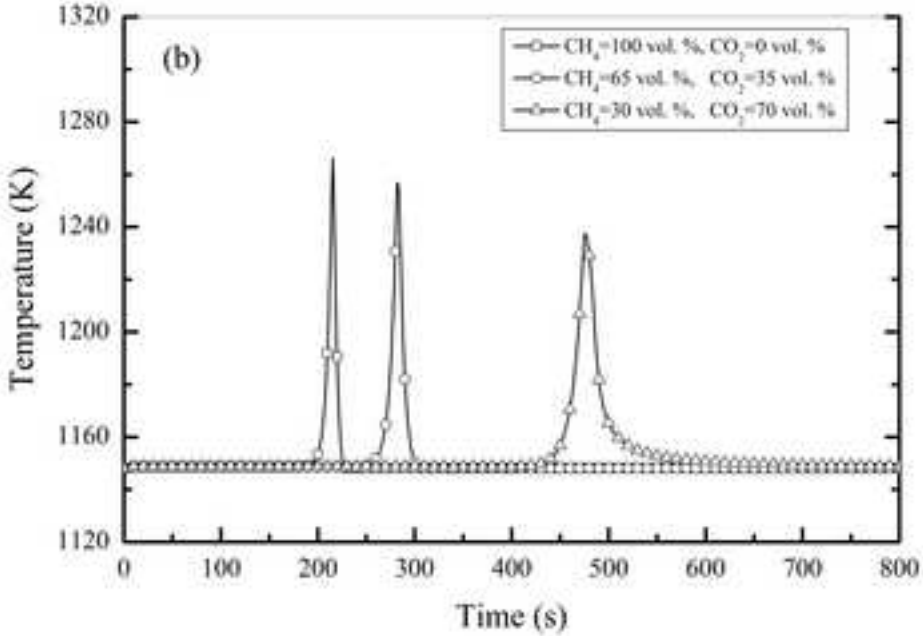

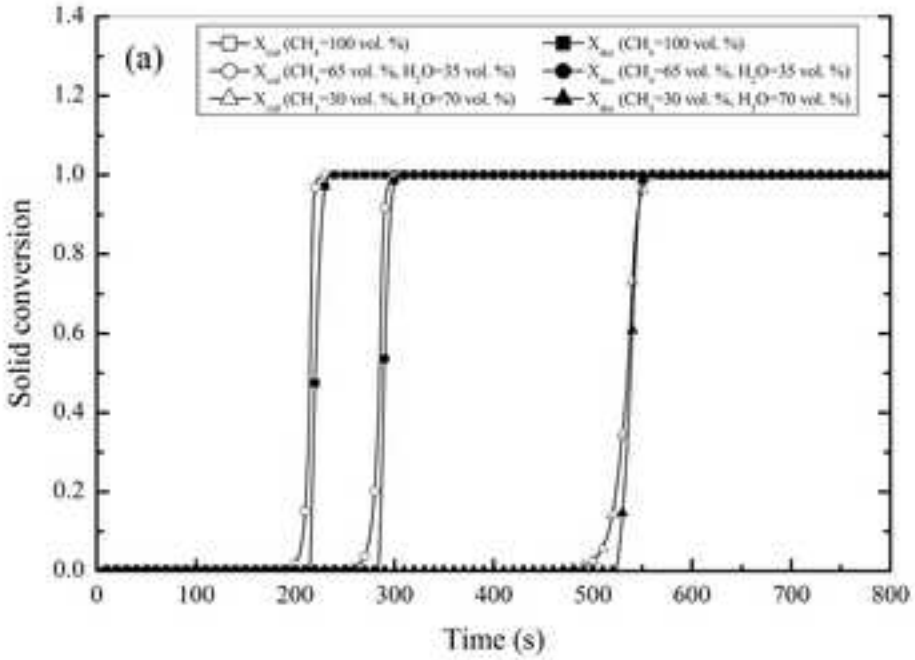

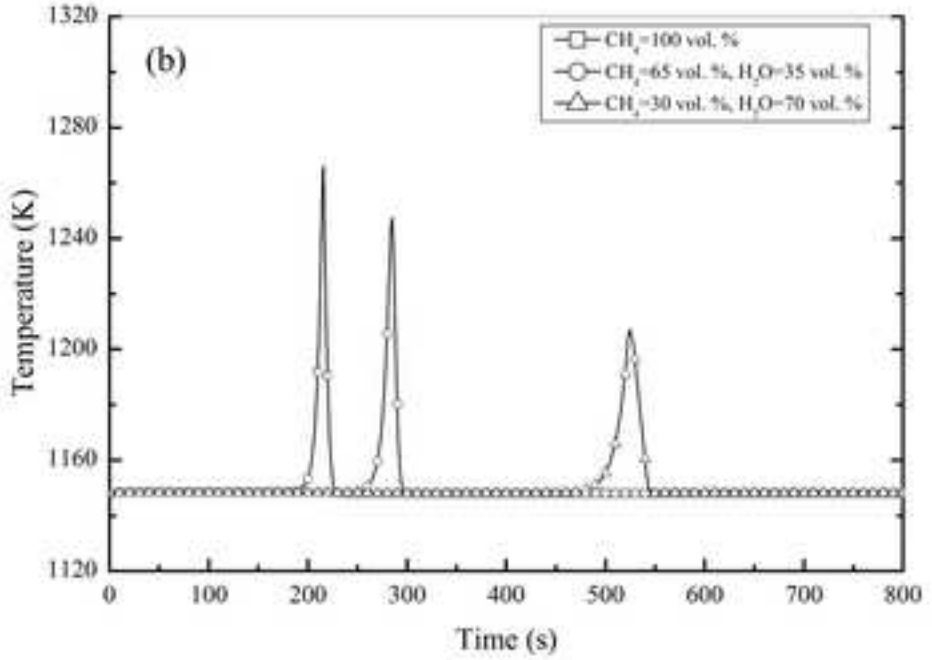

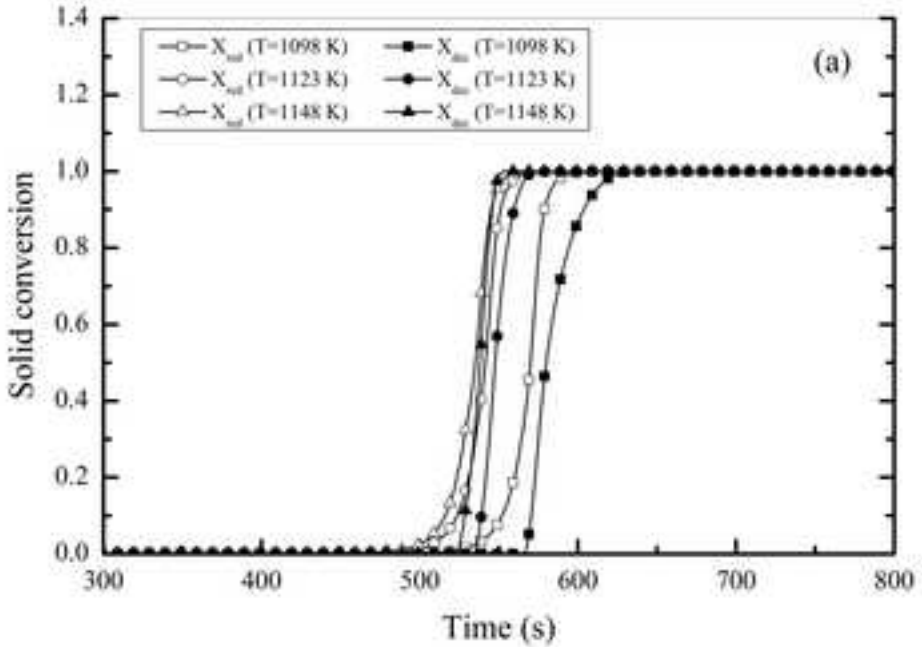

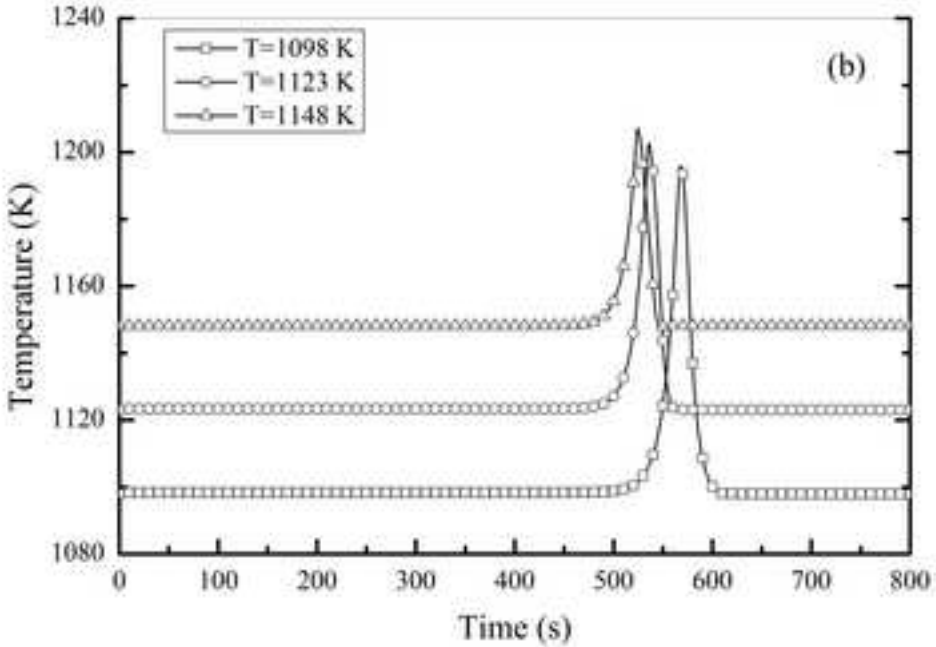

Highlights

- Dynamic model describing the calcination process in CaL-CLC was proposed.
- Calcination data under conditions of interest for CaL-CLC were obtained.
- Reduction of CuO with CH_4 is sufficiently fast under the conditions of interest.
- Addition of steam is helpful in achieving matching kinetics for the two reactions.